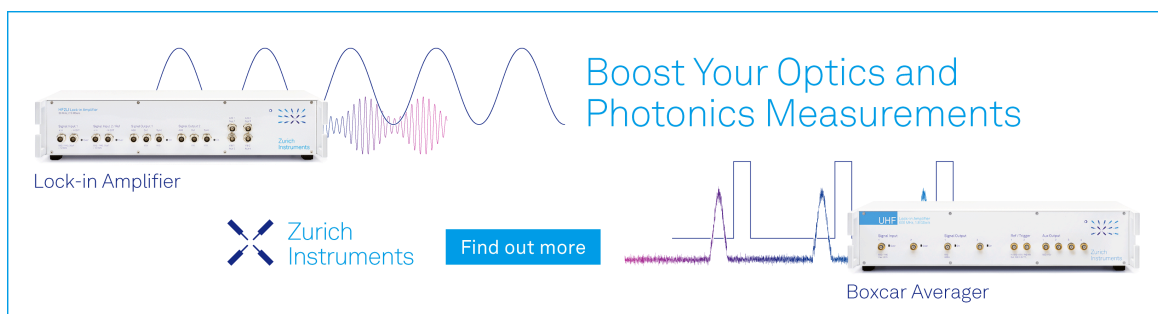# Kinetics of stepwise nitrogen adsorption by size-selected iron cluster cations: Evidence for size-dependent nitrogen phobia

Annika Straßner ; Matthias P. Klein ; Daniela V. Fries ; Christopher Wiehn; Maximilian E. Huber ;
Jennifer Mohrbach; Sebastian Dillinger; Dirk Spelsberg; P. B. Armentrout ; Gereon Niedner-Schatteburg

Check for updates

View Online   Export Citation

Kinetics of stepwise nitrogen adsorption by size-selected iron cluster cations: Evidence for size-dependent nitrogen phobia

View Online   Export Citation   CrossMark

Annika Straßner,[1] Matthias P. Klein,[1] Daniela V. Fries,[1] Christopher Wiehn,[1] Maximilian E. Huber,[1] Jennifer Mohrbach,[1] Sebastian Dillinger,[1] Dirk Spelsberg,[1] P. B. Armentrout,[2] and Gereon Niedner-Schatteburg[1,a]

AFFILIATIONS

[1] Fachbereich Chemie and Forschungszentrum OPTIMAS, Technische Universität Kaiserslautern, 67663 Kaiserslautern, Germany
[2] Department of Chemistry, Univerdstsity of Utah, Salt Lake City, Utah 84112, USA

a)Author to whom correspondence should be addressed: gns@chemie.uni-kl.de

ABSTRACT

We present a study of stepwise cryogenic N_2 adsorption on size-selected Fe_n^+ (n = 8–20) clusters within a hexapole collision cell held at T = 21–28 K. The stoichiometries of the observed adsorption limits and the kinetic fits of stepwise N_2 uptake reveal cluster size-dependent variations that characterize four structural regions. Exploratory density functional theory studies support tentative structural assignment in terms of icosahedral, hexagonal antiprismatic, and closely packed structural motifs. There are three particularly noteworthy cases, Fe_{13}^+ with a peculiar metastable adsorption limit, Fe_{17}^+ with unprecedented nitrogen phobia (inefficient N_2 adsorption), and Fe_{18}^+ with an isomeric mixture that undergoes relaxation upon considerable N_2 uptake.

I. INTRODUCTION

The investigation of transition metal (TM) clusters and their ligation is a field of significant importance. The structural similarities of such clusters to catalytically active surfaces justify a quest for enhanced knowledge of cluster structure and properties.[1-5] Such knowledge might enable the rational design of improved catalysts for industrial use. Gas phase clusters serve as model systems for active sites on surfaces, and they provide for a cluster-size dependent tuning of metal mediated chemistry.[2,6]

Early cluster studies reveal significant changes with the cluster size in their chemical and physical properties, which level off toward the bulk limit according to scaling laws.[7-14] Particularly, iron clusters show a strong size effect in their reactions with small molecules; numerous experimental and theoretical studies document the gas-phase reactivity of negatively charged, neutral, and positively charged Fe_n clusters with small diatomic molecules, such

as H_2,[8,9,15-17] D_2,[18,19] N_2,[20] O_2,[21,22] and CO,[23,24] as well as the reactivity with larger molecules, such as ammonia,[8,25-29] water,[8,30,31] carbon dioxide,[32] ethene,[33] and benzene.[34-36]

Although often obedient to scaling laws, iron clusters allow themselves singular exceptions, which are often coined "magic numbers" that tentatively relate to particular structural motifs. For example, the mass spectra of Fe_n^+ reveal a sequence of magic numbers n = 7 (pentagonal bipyramid), 13 (icosahedron), 15 (bcc motif), and 19, 23 (polyicosahedron).[37] Neither assumptions regarding electronic shell closures[38] nor packing of hard spheres[39] help to explain these magic numbers. In remarkable contrast, collision-induced dissociation (CID) experiments do verify enhanced stabilities of the listed "magic numbers," n = 7, 13, 15, and 19 for ionic and neutral iron clusters.[40] Spin-polarized density functional theory (DFT) calculates high stabilities of small iron clusters with 7, 13, and 15 atoms and indicates the important role of magnetism in determining stabilities and magic numbers.[41]

A. Magnetism

The magnetism of small iron clusters is of interest by itself. The average magnetic moments per atom of neutral iron clusters as determined by Stern–Gerlach experiments are enhanced with respect to those of bulk iron.[42,43] Small cluster ferromagnetism below 30 atoms is atom-like. The magnetic moments of large clusters approach the bulk limit, whereas some oscillations might relate to surface-induced spin-density waves, likely indicating some spin relaxation.[42,44] Cryogenic homonuclear iron clusters Fe_n exist in two states with distinct magnetic moments μ, indicating distinct valences and metastability. The interpretation concluded there was Heisenberg-like ferromagnetism with a ground state configuration $3d_\uparrow^5 3d_\downarrow^2 4s^1$ (S = 3/2) yielding a magnetic moment of 3 μ_B/atom and an excited state with $3d_\uparrow^4 3d_\downarrow^3 4s^1$ (S = 1/2) yielding a magnetic moment of 1 μ_B/atom. A Falicov–Kimball model serves to explain metastability and near degeneracy of both states. Of course, non-scalable cluster size effects are much beyond such a simplified approach.[45]

The Fe_{13}^+ cluster has drawn special attention because of its anomalously low magnetic moment that arises from antiferromagnetic coupling of the central atom to the atoms in the surrounding shell.[46] There is some controversy whether the low magnetic moment manifests a symmetry-driven quenching of the local spin moments of all cluster atoms with some larger quenching of the central atom.[47] Another DFT study found a magnetic transition upon ionization, namely, from a ferromagnetic-like configuration to an antiferromagnetic one with some T_h-deformation.[48] Other icosahedral metal clusters M_{13} received considerable attention in various contexts.[49–53]

B. Further quantum chemical modeling

The inseparable structure—magnetism—stability relationship imposes a significant challenge for the quantum chemical modeling of Fe_n clusters. Early on, such studies revealed the tendency of Fe clusters toward extended bond lengths, narrower d-band widths, and maximum pairs of nearest-neighbor bonds, all of which maximize ferromagnetic stability.[54] In contrast, the most stable small Fe_n structures evaluated with DFT and molecular dynamics simulations in other studies are compact with short bond lengths below bulk values—but agree on high magnetic moments ≈ 3 μ_B/atom,[55,56] as confirmed elsewhere.[57] Some structural magnetic discontinuities are predicted for Fe_n at $n = 6$ and $n = 10$.[58]

A more recent systematic DFT survey of Fe_n, Fe_n^-, and Fe_n^+ ($n = 7$–20) obtained ionization energies, vertical electron detachment energies, binding energies, and total magnetic moments that nicely reproduce the published experimental findings. Charge states and sizes modulate the obtained icosahedral structural motifs with indications of distorted hexagonal antiprismatic structures for $n = 14$ and beyond, coming back to capped icosahedral structures at $n = 19$.[59] Further studies confirm this geometrical evolution, and they manage to predict further experimental values, such as magnetic moments, ionization energies, electron affinities, fragment energies, and polarizabilities.[24,60,61] Further advanced modeling deals with noncollinear magnetism, which is beyond the scope of the current study.[62–64]

C. Catalytic N₂ activation

The physisorption and chemisorption of N_2 on metal surfaces have been a topic of considerable interest[65] because of its intimate connection with many catalytic processes, notably the Haber–Bosch process for ammonia production. Extensive investigations on TM clusters have been conducted to enable N_2 fixation under mild conditions and to elucidate efficient processes of N_2 activation and transformation.[66–68] It is assumed that the rate-determining step in the industrial ammonia synthesis is the dissociation of N_2 using iron as a catalyst.[69,70] The equivalent bottleneck in enzymatic N_2 activation is its fixation by the nitrogenase enzyme at room temperature.[71]

D. N₂ adsorption on Fe surfaces

In the context of industrial N_2 activation and enzymatic activation, it is the initial adsorption that precedes and likely directs the activation. Iron catalyzes the breaking of the strong N–N triple bond. It has been shown experimentally that N_2 adsorption on the Fe(111) surface takes place either in α-N_2 motif (strongly inclined to the surface) or in a γ-N_2 motif (perpendicular to the surface), as elucidated by angle resolved photoelectron spectra and *ab initio* generalized valence bond calculations.[72] Further spectroscopic studies of N_2 adsorbed on the Fe(111) surface refined these findings and revealed three characteristic α-, β-, and γ-states, which refer to side-on chemisorption (α), head-on chemisorption (γ), and dissociative chemisorption (β) to the metal surface atoms.[65,73] Calculations identified two dissociation channels, one with a low energy barrier but a high entropy barrier and one highly activated "direct channel" with a completely new precursor state.[74] A subsequent DFT study predicted that the most favorable N_2 adsorption occurs on a quadruple hollow site, such as that on a Fe(110) surface.[75] Early combined matrix isolation and DFT studies of $Fe_{1,2,3}(N_2)_n$ complexes concluded that there was a strong preference for N_2 end-on coordination in the ground state species.[76,77] Recent DFT calculations have modeled iron nitride cluster coalescence and concomitant total spin reduction.[78]

E. IR spectroscopy of iron cluster adsorbate complexes

Exclusively dissociative H_2 adsorption to Fe_n^+ clusters yields hydride clusters, and their IR spectroscopic characterization reveals twofold or threefold coordinated hydrides, whereas extended metal surfaces prefer exclusively high coordination, threefold or higher, when migrating into the bulk.[79] Somewhat surprisingly, water hydrolysis by cationic Fe clusters increases with cluster size.[80]

F. Our previous work of relevance

The University of Utah laboratory has examined the chemistry of iron cluster cations using guided ion beam tandem mass spectrometry (GIBMS) instrumentation. These include a determination of the cluster binding energies by collision-induced dissociation (CID) with Xe.[40,81] Further studies examined reactions of Fe_n^+ with D_2 ($n = 2$–15),[19] O_2 ($n = 2$–18),[22] CO_2 ($n = 1$–18),[32] and CO ($n = 1$–17).[23] CID studies of $Fe_mO_n^+$ ($m = 1$–3, $n = 1$–6)

provided additional thermochemistry for these small iron oxide cluster cations.[21] Of direct relevance to the present work, reactions of Fe_n^+ (n = 1–19) with N_2 were examined and Fe_n^+–N and Fe_n^+–2N bond energies were measured.[20] An activation barrier of 0.48 ± 0.03 eV was determined for activation of N_2 by the larger clusters (n = 12, 15–19). Fe_n^+–N bond energies were also determined in reactions with ND_3 (n = 2–10, 14).[29]

G. TUK studies

In complement to these GIBMS studies at the University of Utah, the Technische Universität Kaiserslautern (TUK) laboratory utilizes a tandem cryo ion trap instrument,[82,83] which allows the study of the adsorption and reaction kinetics of clusters under single collision conditions at temperatures down to 11 K as well as Infrared Photon Dissociation (IR-PD) spectroscopy. Prior studies of cationic nickel clusters established a concept of rough and smooth cluster surfaces,[84] and the combination of N_2 adsorption kinetics and IR spectroscopy allowed for systematic refinement of cluster size dependencies and structural changes.[85] The concept proved transferable by application to cationic rhodium clusters[86] and cationic cobalt clusters.[82] N_2 and H_2 coadsorption on cationic ruthenium clusters yielded distinguishable IR fingerprints when changing the sequence of adsorptions.[87] Most recently, cationic tantalum clusters were investigated for their potential for N_2 activation, and a multidimensional path for N_2 cleavage was identified as an *across edge-above surface* (*AEAS*) mechanism.[88] Complementary investigations by gas phase X-ray Magnetic Circular Dichroism (XMCD) have characterized the spin and orbital contributions to the magnetic moments of Fe, Co, and Ni cluster cations.[14,89]

In this work, N_2 adsorption onto cationic iron clusters $[Fe_n(N_2)_m]^+$ (n = 8–20) is elucidated by kinetics investigation under single collision conditions. Strong support of the present findings are obtained through our complementary cryogenic infrared spectroscopy study,[90] which we will refer to in the following as **[IRS]**. The combined studies provide insight into the metal–adsorbate bonding and unravel structure–reactivity relationships and their variations with cluster sizes.

II. EXPERIMENTAL AND COMPUTATIONAL METHODS

A customized Fourier Transform Ion Cyclotron Resonance (FT-ICR) mass spectrometer (Apex Ultra Bruker Daltonics) was used to perform all the experiments. The Fe clusters were generated by a home-built laser vaporization cluster ion source (LVAP), as described before.[91,92] The iron atoms were evaporated from a rotating 0.4 mm thick isotopically enriched ^{56}Fe foil (99.93%, Oak Ridge National Laboratories) using the second harmonic of a pulsed Nd:YAG laser (Innolas *Spitlight 300*, 20 Hz). The resulting hot plasma was captured by a He gas pulse (40 μs, 15 bars) created by a homebuilt piezoelectric valve.[93] The atoms and ions in the plasma cooled down and aggregated to clusters in the subsequent jet expansion through a 69 mm long channel (Ø 2 mm) into vacuum (10^{-7} mbar). The cluster beam was skimmed, and after passing a 90° ion beam bender, the clusters were mass selected using a quadrupole mass filter and injected into a cryogenic hexapole ion trap. The ion trap was cooled to 26 K by a closed cycle He cryostat. To achieve sufficient nitrogen attachment, the pressure in the

ion trap was increased from 1.2×10^{-7} mbar up to a maximum of 5.0×10^{-7} mbar. To accomplish efficient trapping and cooling of the ions, additional helium was introduced and the pressure increased to 4.0×10^{-6} mbar. The buffer and the reaction gas were introduced continuously. After storing the mass-selected ions for various times (0–15 s), the cluster adsorbate complexes of the form $[Fe_n(N_2)_m]^+$ = (n, m) were guided by electrostatic lenses into the FT-ICR cell. The ICR uses a so-called "infinity" type[88] cell, which was held at temperatures below 10 K with a closed cycle He cryostat to prevent heating of the clusters by black-body radiation. The ICR cell was used to isolate and detect the formed $[Fe_n(N_2)_m]^+$ = (n, m) cluster adsorbate complexes.

To investigate the cationic iron clusters and their nitrogen adducts, we used adsorption kinetics originating from reaction delay scans. Each recorded mass spectrum consists of an average of 40 mass spectra with fixed hexapole collision cell delays of 0–15 000 ms. We stored the generated $[Fe_n(N_2)_m]^+$ = (n, m) cluster adsorbate complexes in the cryogenic hexapole under isothermal conditions at 26 K. N_2 addition to the Fe cluster cations takes place in bimolecular collisions, where the clusters initially act as their own heat bath. Helium buffer gas collisions start to re-thermalize the cluster adsorbate complexes on a millisecond time scale, while subsequent N_2 collisions and additions take place on a much longer kinetics time scale. Also any radiative stabilization would be much slower. Note that the kinetic energy dependence of Fe_n^+ + CO association reactions was determined before, and these data served to model the bimolecular association processes convincingly over a time scale of 0.1 ms.[23] In the ICR cell, the absence of He buffer gas means that any stabilization of the complexes observed probably occurs by additional collisions with the N_2 gas present, although the longer time scale might also permit some radiative stabilization. This is consistent with the failure to observe these limits for smaller cluster sizes in the ICR cell (see below).

In all the investigated cases (n = 8–20), stepwise N_2 uptake reached an adsorption limit m_{max}. Fitting the experimental data with a pseudo-first-order-kinetic ("evofit" program[94]), we obtained the relative rate constants for N_2 adsorption $k_{(n,m)}$ for each step $m \rightarrow m + 1$ and for N_2 desorption $k_{-(n,m)}$ for each step m + 1 $\rightarrow$ m,

$$[Fe_n(N_2)_m]^+ + N_2 \underset{k_{-(n,m+1)}}{\overset{k_{(n,m)}}{\rightleftharpoons}} [Fe_n(N_2)_{m+1}]^+.$$
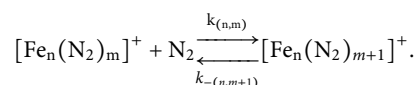
In the following plots, the variation of the background signal (gray area) relates to normalization of varying species intensities. Although these measured data and their fits could be displayed in several ways (Fig. S19), for the following plots, we chose a semi-logarithmic scale.

The absolute rate constants $k_{(n,m)}^{abs}$ are calculated from the relative rate constants $k_{(n,m)}$ with the absolute N_2 gas number densities $\rho_{N_2}(T)$ as the conversion factor,

$$k_{(n,m)}^{abs} = k_{(n,m)}/\rho_{N_2}(T).$$

We obtain approximate values for $\rho_{N_2}(T)$ indirectly from the pressure in the surrounding chamber $p_c^{(300\ K)}$ and an effective geometry factor c_{app},

29 April 2024 06:35:03

$$\rho_{N_2}(26\,\text{K}) = \frac{c_{app}p_c^{300\,\text{K}}}{k_B T_{300\,\text{K}}}.$$

The geometry factor, c_{app}, has a significant temperature dependence and has been evaluated as 1.8 ± 0.4 at 26 K with a net uncertainty of $\pm 50\%$ by numerous kinetic studies of transition metal cluster cations with neutral reactants at cryogenic temperatures.[85]

The average dipole orientation theory (ADO)[95,96] extends the classical Langevin collision rate constant of ions with neutrals[97] toward polar molecules and is based on a classical trajectory of a linear dipole in the field of a point charge. The collision rate constant k^{ADO} gives the theoretical limit of the absolute rate constants,

$$k^{ADO} = \frac{q}{2\varepsilon_0 \sqrt{\mu}}\left(\sqrt{\alpha} + c\mu_D\sqrt{\frac{2}{\pi k_B T}}\right),$$

where q is the charge of an electron, ε_0 is the permittivity of vacuum, μ is the reduced mass of the cluster adsorbate complex, α is the polarizability ($C^2 m^2/J$), μ_D is the dipole moment (D), and k_B is Boltzmann's constant (J/K). The parameter c lies between 0 and 1 and can be expressed by the polarizability volume α' and μ_D.[98] Note that the vanishing dipole moment of N_2 makes k^{ADO} become identical to the Langevin rate constant.

The absolute reaction efficiency γ shows the probability of a reaction occurring after a collision between the cationic iron cluster and the N_2. It is calculated by the quotient of the absolute rate constant (k^{abs}) and the collision rate constant (k^{ADO}).

Kummerlöwe and Beyer introduced two models for calculating the collision rate constants of ionic clusters with neutral molecules: the hard sphere average dipole orientation model (HSA) and the surface charge capture model (SCC).[99] In both models, the cluster and the neutral reaction partner are assumed as hard spheres, and the charge is assumed as point charge. The difference is in the location of the charge. For the HSA model (k^{HSA}), the charge is located in the center of the cluster, while in the SCC model (k^{SCC}), the charge is freely movable but changes to the cluster surface during the attractive interaction with the neutral, polarizable collision partner.

III. RESULTS AND DISCUSSION

A. Molecular nitrogen adsorption on iron cluster cations: Trends and limits of adsorption

We have investigated the trapped $[Fe_n(N_2)_m]^+ = (n, m)$ clusters in the cryogenic hexapole trap under isothermal conditions at 26 K. We find a successive stepwise gain of +28 m/z as the trapping time is increased. The recorded mass spectra of the exposed Fe_n^+ cluster ($n = 8\text{--}20$) species thus reveal stepwise adsorption of molecular nitrogen.

N_2 uptake seems to reach limits beyond which further increases of N_2 pressure (up to 5×10^{-7} mbar) and/or trapping–exposure time (beyond 20 s) do not lead to a further increase in N_2 uptake by the iron clusters. In order to quantify this phenomenon, we define an adsorption limit by the particular value m_{max} of the largest detectable complex (n, m) as obtained by our setup.

Of course, there is always a dynamic adsorption/desorption equilibrium $(n, m_{max}) \rightleftharpoons (n, m_{max+1})$. However, this equilibrium is clearly on the side of (n, m_{max}), and (n, m_{max+1}) does not populate. The forward rate constant $k_{m_{max}}$ is slow, the backward rate constant $k_{-m_{max+1}}$ is fast, and their ratio is large, which means that the equilibrium constant is small, and thus, the Gibbs energy $\Delta_r G^0(n, m_{max})$ of adsorption diminishes. In the recorded data, we find cases where the $(n, m_{max-1}) \rightleftharpoons (n, m_{max})$ equilibrium is on the side of m_{max} [Fig. 1(a)], and we find cases where it is on the side of m_{max-1} [Fig. 1(b)].

Beyond such adsorption limits m_{max}, we find some cases with retardation in the uptake of N_2 $(n, m^*) \rightleftharpoons (n, m^* + 1)$ at particular values m^*, which therefore become the most intense cluster adsorbate species. In four cases, $n = 11, 12, 18,$ and 19, we observe $m^* = m_{max}$ [e.g., Fig. 1(a)]; in another four cases, $n = 8, 9, 10,$ and 20, we find $m^* = m_{max-1}$ [e.g., Fig. 1(b)]; and there are three further cases, $n = 14, 15,$ and 16, (17), where $m^* = m_{max-2}$. The $n = 13$ cluster is a special case where $m^* = m_{max-6}$. In Table I, we list m^* only for those cases where it differs from m_{max}. Beyond these effects at or close to saturation of N_2 adsorption, we find additional kinetic retardation of N_2 uptake at much lower levels of N_2 coverage of Fe cluster species. We list such findings as metastable adsorption limits m_x.

The thus defined three types of particular adsorbate levels, m_{max}, m^*, and m_x, serve as guidelines for some elucidation of adsorbate bonding and cluster geometries. Notably, $m_{max} : n \leq 1$ in all investigated cases, $n = 7\text{--}20$ (Fig. 2). We recognize four characteristic regions of (n, m_{max}) stoichiometries: small clusters, $n = 7$ and 8, reveal $m_{max} = n$; mid-size clusters, $n = 9\text{--}13$, reveal $m_{max} = n - 1$; and large clusters, $n = 18\text{--}20$, reveal $m_{max} = n - 2$. Beyond these seemingly clear cases, there is a somewhat strange region of intermediate clusters, $n = 15\text{--}17$, where $m_{max} = n - 8$. The sole case of $(14, 8)$, which is $m_{max} = n - 6$, falls in between the mid-size cluster $m_{max} = n - 1$ region and the intermediate cluster region of $m_{max} = n - 8$.

In order to verify the found anomalies, we repeated our cryo absorption experiments within the FT-ICR MS analyzing and trapping cell. This allows for a controlled variation of conditions in multiple regards (cf. Table S1 in the supplementary material). We found identical m_{max} results for $n = 16\text{--}19$ (Fig. 2, gray dots) as in the experiments that took place within the RF hexapole trap. For smaller clusters, $n \leq 15$, adsorption was too slow to reach m_{max}, presumably because there are insufficient thermalizing collisions in the ICR cell.

Some structural speculation seems possible. Regarding N_2 adsorption as a molecular titration of atomic surface binding sites—the ground-paving Langmuir picture—the results of Fig. 2 suggest that the small clusters ($n = 7$ and 8) possess "surface only" type structures, void of inner Fe atoms. Thus, each surface atom adsorbs a single N_2 and $m_{max} = n$. Mid-size clusters ($n = 9\text{--}13$) appear to possess a single Fe atom that is not accessible for N_2 adsorption. Thus, $m_{max} = n - 1$. Candidate structures include an $n = 13$ icosahedron and structures of smaller clusters that derive from it. In such cases, e.g., $n = 11$ and 12, the former "inside" Fe atom starts to obtain some exposure to the outside, albeit by a shallow concave pocket. Apparently, N_2 does not coordinate to this semi hidden atom. Computed candidate structures for $n = 9$ and 10[95] do not reveal such a concave pocket. All Fe atoms are
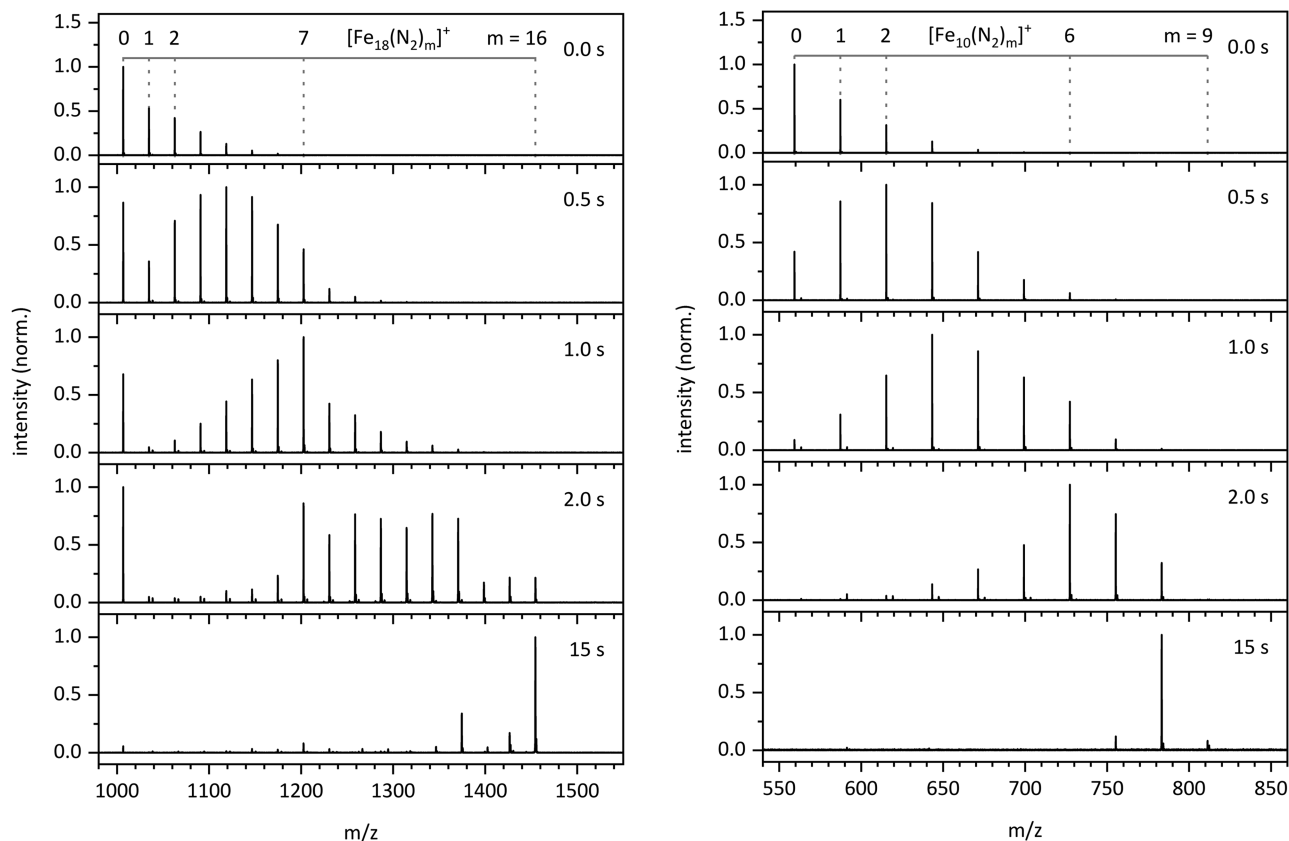
29 April 2024 06:35:03

FIG. 1. Temporal evolution of the mass spectra of mass-selected $Fe_{18}^+ = (18, 0)$ clusters (the left stack) and of mass-selected $Fe_{10}^+ = (10, 0)$ clusters (the right stack). In both cases, the clusters are exposed to 2.1×10^{-7} mbar of N_2 in 3.8×10^{-6} mbar of He at 26 K for up to 15 s. Note the adsorption limits $m_{max} = 16$ and $m_{max} = 9$ and their relative intensities, the metastable adsorption limit $(n, m_x) = (18, 7)$, and the most intense cluster adsorbate complex $(n, m^*) = (10, 8)$. Minor peaks +4 amu beyond those of N_2 adsorbates signify single O_2 adsorbates which stem from residual O_2 background gas.

exposed and seem approachable from the outside by prospective adsorbates; however, both of these candidate structures possess a sole Fe atom that is eightfold coordinated to the next neighbor Fe atoms—with only fourfold to sixfold coordination of all the other Fe atoms.

Large clusters ($n = 18$–20) may continue with icosahedral binding motifs. A double icosahedron was predicted for $n = 19$.[95] Related structures may be derived by addition of a single capping atom or by removing a single atom, accompanied by some structural relaxation. In any case, we obtain candidate structures for $n = 18$–20 with two internal atoms that are not accessible to any adsorbates such that $m_{max} = n - 2$ behavior seems reasonable. Of course, it is conceivable—and in part likely—that a multitude of N_2 adsorbates could induce structural relaxation of the hosting surface.

In any case, the intermediate region, $n = 14$–17, corresponds to none of these trends nor to the above structural arguments; its $m_{max} = n - 8$ behavior seems strange in terms of structural categories. This deems likely an alternative explanation in terms of electronic properties, and it is worthwhile to elucidate this phenomenon further.

B. Temperature dependence of the N_2 adsorption

We varied the cryo temperature of our RF hexapole trap within reasonable margins (21–28 K) in steps of 1 K and re-recorded adsorption limits for m_{max} of N_2 on Fe_n^+ clusters, $n = 8$–20 (Fig. 3). Note that in these experiments, we took care to stabilize the partial pressures within the RF hexapole trap to constant values, $p(N_2) = 2.4 \times 10^{-7}$ mbar and $p(He) = 3.6 \times 10^{-6}$ mbar, while we varied the N_2 pressure in the previous experiments (Fig. 2) as appropriate to achieve ultimate maxima of adsorption.

Besides the many details of these data, we find the general trend of high N_2 adsorbate loads at temperatures of 24 K and above and low N_2 loads below 24 K. This observation (from isothermal buffer gas experiments) is opposite to the expected equilibrium behavior of a rigid adsorber: Rising the temperature should ordinarily shift an adsorption/desorption equilibrium toward desorption. Instead, the higher temperature seems to assist in some kind of activation that allows for enhanced N_2 uptake—up to 26 K where we find the largest amounts of N_2 uptake. In the cases of some Fe_n^+ clusters, $n = 8$–10 and 15–17, the adsorption limit decreases somewhat in the 27 K and 28 K experiments. Note that we did take care in reproducing all of

TABLE I. Recorded adsorption limits m_{max}, most intense cluster adsorbate complexes m^*, and metastable adsorption limits m_x of N_2 adsorption on cationic Fe clusters Fe_n^+, $n = 8$–20, in the RF hexapole trap at 26 K. For the corresponding graph, see Fig. S1 in the supplementary material.

Cluster size	Number of adsorbed N_2		
n	m_x	m^*	m_{max}
8	4	7	8
9		7	8
10		8	9
11			10
12	7		11
13	4	6	12
14	4	6	8
15	2	5	7
16	3	6	8
17	4[a]	7[a]	9
18	7		16
19	9		17
20	11	17	18

[a]We extrapolate these numbers from experiments at two times higher N_2 partial pressure.

our findings by multiple independent runs of experiments throughout an extended period of time (of more than one year). We found full verification of these two trends with minor variations in absolute N_2 uptake counts.

Superimposed on these trends, there are interesting variations for particular size-selected Fe_n^+ clusters. Most remarkable, the Fe_{17}^+

cluster shows an extremely pronounced temperature dependence of N_2 uptake, which seemingly vanishes at 22 K and remains meager by amount and intensity at 21 and 23 K. We provide extended plots of temperature dependences in the supplementary material (Figs. S6–S18).

C. Isothermal kinetics under cryogenic conditions

We further investigated the stepwise N_2 adsorption on Fe_n^+, $n = 8$–20, clusters by recording their reaction kinetics in more detail, and we performed pseudo-first-order kinetic fits by our genetic algorithm routine.[94] The kinetic fits confirm consecutive N_2 adsorption steps. The signals for all but one Fe_n^+ cluster reactant decay mono exponentially without any indication of a second isomeric component. This result allows us to fit each consecutive adsorption step by a single rate constant. In some cases—to be discussed below—the recorded data require fitting with inclusion of significant desorption reactions in order to achieve converged fits. The N_2 adsorption to Fe_{18}^+ is the single exception, which exhibits a clear biexponential decay in the initial adsorption step and thus reveals a more involved scheme of N_2 interactions.

1. $Fe_8^+ + N_2$—An all surface Langmuir type $m_{max} = n$ case

In the case of (8, m), we had observed a metastable adsorption limit m_x at (8, 4), a most intense cluster adsorbate complex m^* at (8, 7), and the adsorption limit m_{max} at (8, 8). There are a few published DFT studies of cationic Fe_8^+ that have predicted a bisdisphenoid structure.[59,61] One may expect that the next neighbor coordination of each of the Fe atoms modulates their functionality to
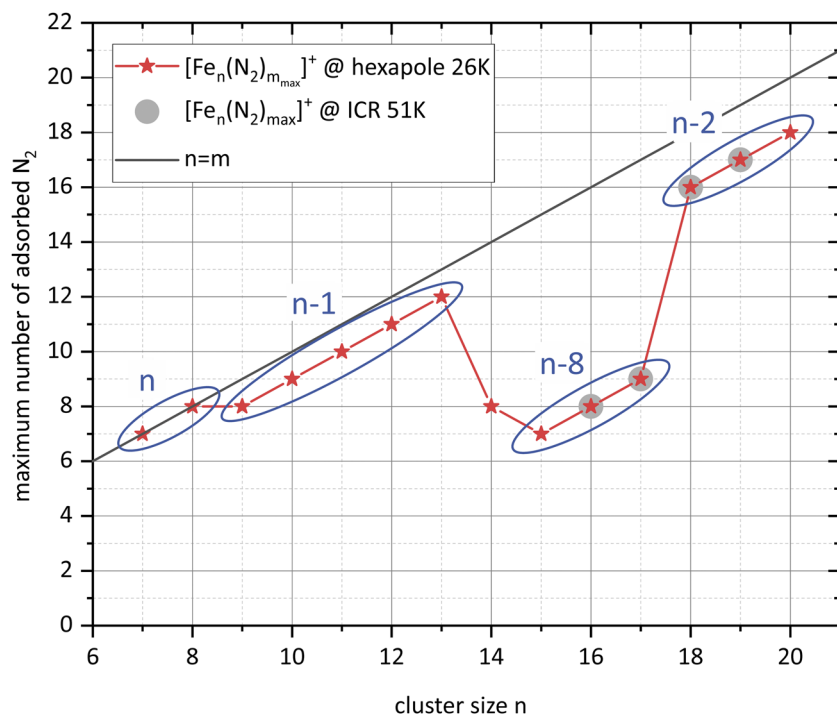

FIG. 2. Adsorption limits m_{max} of N_2 adsorption on cationic Fe clusters Fe_n^+, $n = 6$–20, as recorded in the RF hexapole trap at 26 K in 3.6×10^{-6} mbar He buffer gas (red stars) and as recorded in the ICR cell at 51 K (gray dots). The black line stands for a 1:1 stoichiometry of N_2 and Fe ($n = m_{max}$). Mass-selected Fe_n^+ clusters were stored for up to 20 s and under exposure of up to 5×10^{-7} mbar N_2 at maximum, with saturation typically being reached at lower pressures. Note the indicated regions of different stoichiometries.
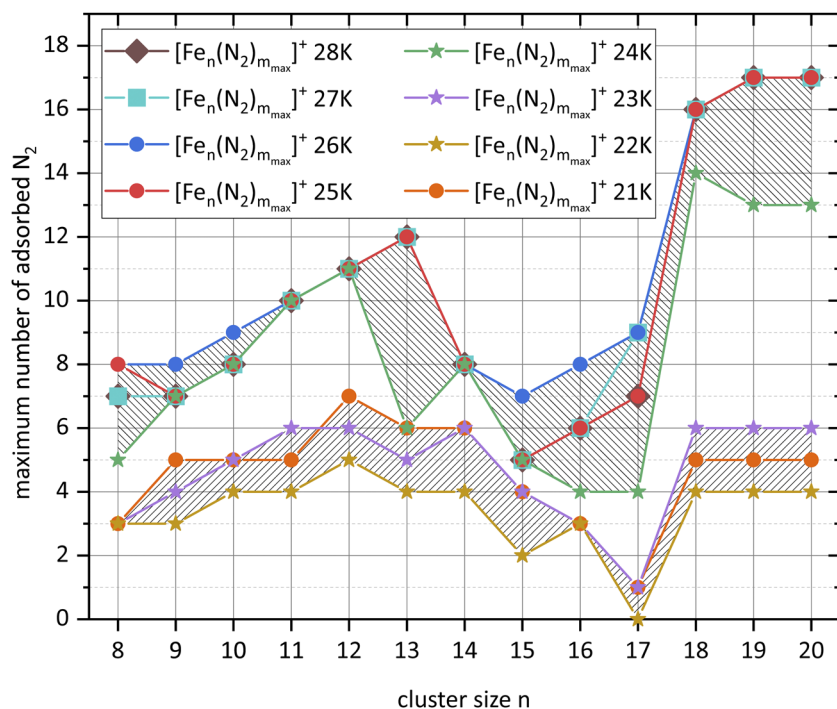
29 April 2024 06:35:03

FIG. 3. Recorded N_2 adsorption limits m_{max} on Fe_n^+, $n = 8$–20, at 21–28 K when exposed for 15 s to 2.4 × 10^{-7} mbar of N_2 in 3.6 × 10^{-6} mbar He buffer gas. In general, the extent of N_2 adsorption decreases by lowering the temperature, and it shows a remarkably strong dependence on the cluster size. Note the diminished N_2 uptake of Fe_{17}^+ at the lowest temperatures. In general, we identify a "high T" regime of high N_2 uptake and a "low T" regime of low N_2 uptake, as emphasized by the shaded areas. These results are reproduced even when doubling the N_2 partial pressure (cf. Fig. S4 of the supplementary material).

act as binding sites for N_2 adsorbates. If so, then a Fe_8^+ cluster with a bisdisphenoid structure—comprising four fourfold and four fivefold coordinated Fe atoms—would lead to changes in consecutive N_2 adsorption at stoichiometries of (8, 4) and (8, 8). Our

recorded kinetic data are not in line with these predictions. DFT modeling of neutral Fe_8 clusters find either a capped pentagonal bipyramid[24,60,64,100] or a bisdisphenoid structure.[57–59,64] A capped pentagonal bipyramid Fe_8^+ would provide for one threefold, three
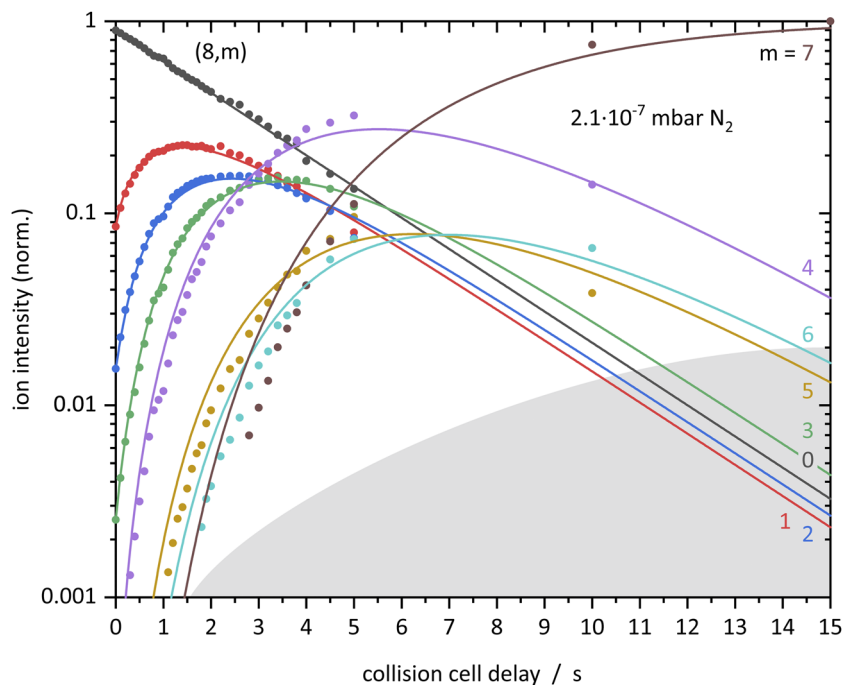

FIG. 4. Isothermal kinetics of the stepwise N_2 adsorption by the isolated Fe_8^+ cluster within 4.0 × 10^{-6} mbar He buffer gas and 2.1 × 10^{-7} mbar of N_2 (solid dots) at 26 K. The pseudo-first-order kinetic fits (solid lines) reveal reaction chains of up to seven consecutive steps.

fourfold, three fivefold, and one sixfold coordinated Fe atoms, all of which are located at the cluster surface and are accessible for adsorbates. Initial N_2 adsorption to the threefold and fourfold coordinated Fe sites and additional adsorption to the fivefold coordinated Fe atoms would result in changes in consecutive N_2 adsorption at stoichiometries (8, 4) and (8, 7). Such an assumption does indeed correlate well with the observed m_x and m^* values. The last adsorption step k_7 (cf. Fig. S34 and Table S15)—yielding the (8, 8) complex—might occur to the sixfold coordinated Fe site. We observe this step being very slow and leading to a very low intensity of the (8, 8) product complex (Fig. 4). Both of our findings appear to relate well to the high next neighbor coordination of this last Fe adsorption site.

2. Fe_9^+ – Fe_{13}^+ + N_2—the $m_{max} = n - 1$ cases reveal center atom inclusion

In the range of $n = 9$–13, we see stepwise N_2 adsorption up to an adsorption limit m_{max} of $n - 1$ N_2 molecules. In particular, the case of (9, m) reveals an adsorption maximum m_{max} at (9, 8) and a most intense cluster adsorbate complex m^* at (9, 7). Likewise, the (10, m) case reveals m_{max} at (10, 9). The most intense cluster adsorbate complex m^* at (10, 8) is in equilibrium with m_{max} and (10, 7). The fitted rate constants of N_2 adsorption show little step-by-step variation with a slight decline that increases steeply toward m_{max} (Fig. 5). Their values are documented in the supplementary material (cf. Figs. S35 and S36 and Tables S16 and S17).

The reported most stable structures for neutral Fe_9 and Fe_{10} clusters correspond to capped square antiprisms or to capped trigonal or capped pentagonal bipyramid motifs.[24,58,60,61,64,100] These geometries would lead upon further growth by stepwise addition of

Fe atoms to the predicted icosahedral structure of neutral Fe_{13}.[24,60,64] Two DFT studies of cationic Fe_9^+ and Fe_{10}^+ clusters[61,100] predict capped pentagonal bipyramidal motifs. The Fe_9^+ bicapped pentagonal bipyramidal structure consists of four fourfold, one fivefold, two sixfold, and one eightfold coordinated Fe atoms, and the cluster surface has an all convex shape. The Fe_{10}^+ tricapped pentagonal bipyramidal structure consists of three four-, five-, and sixfold and one ninefold coordinated Fe atoms, and the cluster surface is all convex except for a shallow concave pocket at the ninefold coordinated Fe atom. In both cases, the single high-coordinated Fe atom might possess a lower N_2 adsorption enthalpy than all of the lower coordinated Fe atoms. If so, this might induce adsorption maxima $m_{max} = n - 1$ as observed.

In addition, the adsorption maximum m_{max} at (10, 9) reveals a dynamic adsorption/desorption equilibrium with the $m^* = n - 2$ complex (10, 8) and with (10, 7)—with the (10, 9) kinetic curve barely above the noise level. Similar behavior occurs for the $n = 9$ case at elevated pressures. This behavior is beyond an interpretation in merely structural terms. Instead enthalpic and entropic reasoning seems operational. It might be that the three sixfold Fe sites do not adsorb strongly.

The (11, m) case reveals an adsorption limit m_{max} at (11, 10) in equilibrium with its precursor (Fig. 6 left). The rate constants of stepwise N_2 adsorption are similar to the (9, m) and (10, m) cases, and they show little variation up to m = 7. In line with our previous studies of N_2 adsorption on Ni_n^+ clusters,[84] we identify this as an indication for a *smooth* cluster surface of many equivalent adsorption sites. The rate constant $k_{(11,8)}$ for the ninth adsorption step significantly diminishes by more than a factor of two. The final, ninth step reveals further reduced adsorption in equilibrium with desorption (cf. Fig. S37 and Table S18).
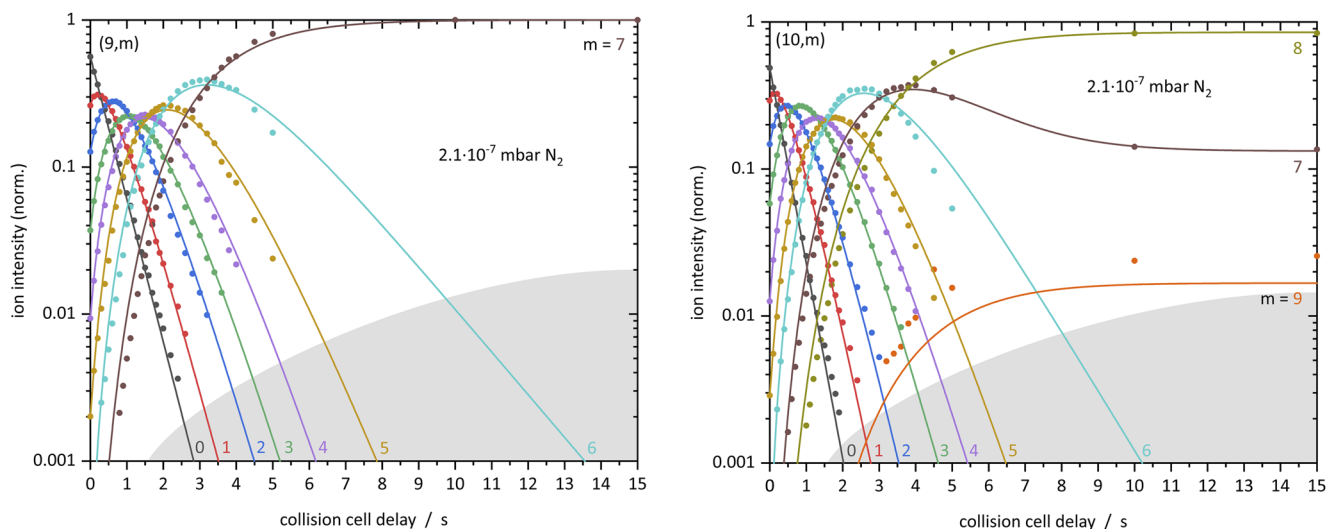
FIG. 5. Isothermal kinetics of the stepwise N_2 adsorption by isolated Fe_9^+ (left) and Fe_{10}^+ (right) clusters within 4.0×10^{-6} mbar He buffer gas and 2.1×10^{-7} mbar of N_2 (solid dots) at 26 K. The pseudo-first-order kinetic fits (solid lines) reveal reaction chains of up to seven and nine consecutive steps.

In the case of (12, m), we find stepwise N_2 adsorption with *roughly* equal rate constants $k_{(12,m)}$ up to the adsorption limit m_{max} at (12, 11) (Fig. 6 right). In particular, there is no decline of adsorption rate constants toward saturation, and there is no indication for any desorption (cf. Fig. S38 and Table S19). Superimposed, we find somewhat retarded N_2 uptake in the eighth and tenth step, $k_{(12,7)}$ and $k_{(12,9)}$, and somewhat enhanced uptake at the ninth step, $k_{(12,8)}$. This behavior leads to a metastable adsorption limit m_x at (12, 7). This observation seems unlikely to find an interpretation in terms of purely structural arguments. Instead, we suggest the possibility of an adsorbate-induced reorganization of the Fe cluster core and/or of the adsorbate layer close to saturation.

Predicted structures of neutral and cationic clusters n = 11, 12 are four- and fivefold capped pentagonal bipyramids, which correspond to incomplete icosahedra.[24,58,61,100] Such a Fe_{11}^+ structure would consist of two fourfold, three fivefold, five sixfold, and one tenfold Fe atoms. The Fe_{12}^+ analog would contain five fivefold, six sixfold, and one elevenfold Fe atoms. In both cases, a single high-coordinated Fe atom would locate in the center of the clusters, shielded against N_2 adsorption. This nicely corresponds to the observed $m_{max} = n - 1$ behavior. Further kinetic details cannot be derived from these structures in an obvious way.

The case of (13, m) is significantly different from all smaller clusters. There is an adsorption limit m_{max} at (13, 12), which excellently points toward an icosahedral structure as predicted before.[24,58,60,61,64,100] The initial adsorption up to m = 6 is fast and stalls at this point; (Fig. 7) the seventh uptake, $k_{(13,7)}$, is slower by two orders of magnitude (Fig. S39 and Table S20). Surprisingly, the next intense larger observable cluster adsorbate complex is (13, 12). We do find very low intensity indications of complexes in between (13, 7) through (13, 11). They may exist merely as adsorbate intermediates. In effect, (13, 6) becomes a metastable adsorption limit m^*. Furthermore, any kinetic fits inevitably need to involve high values of $k_{(13,7)}$ through $k_{(13,11)}$, which rise by a factor of two with respect to the

values of the initial adsorption steps. This significant rise of the adsorption rate constant may originate from some kind of reorganization of the cluster adsorbate complexes in terms of their coupled geometric and electronic parameters. At this point, we can only speculate about details. It is conceivable that the known antiferromagnetic coupling of the central Fe atom in a naked Fe_{13}^+ cluster[46] relaxes under the influence of more than six N_2 ligands. Alternatively, the highly symmetric icosahedral shell of a naked Fe_{13}^+ cluster, which maximizes the amount of next neighbor interactions, starts to break down upon addition of a seventh N_2 ligand, and in effect, there will be lower coordinated Fe centers at the cluster surface that attract further ligands swiftly. Further evidence for the actual mechanism can be found in the accompanying paper on IR spectroscopy and DFT modeling.[90]

3. Fe_{14}^+ – Fe_{17}^+—the $m_{max} = n - 8$ cases reveal adsorption reluctance

The range of Fe_n^+ n = 14–17 clusters has a special adsorption behavior, namely, the initial N_2 uptake is as fast as in all of the other cases—likely close to the collision rate constant and thus with unit efficiency (as discussed below); however, the total amount of uptake is much reduced with respect to the smaller and larger clusters (Fig. 8). This range is therefore labeled as "somewhat reluctant." The n = 15–17 clusters accept n - 8 N_2 molecules at maximum, and the n = 14 cluster accepts $n - 6$ N_2 molecules at maximum.

We find that the rate constant variations up to $k_{(14,7)}$ are identical to that for the case of n = 13 up to $k_{(13,7)}$ (cf. Fig. S40 and Table S21). This is a strong indication that these clusters have similar structures. However, the kinetic fits of Fe_{14}^+ do necessitate a significant amount of desorption, $k_{-(14,7)}$ and $k_{-(14,8)}$, which are absent in the case of Fe_{13}^+. The (14, m) cluster complexes cease to take up any N_2 adsorbates beyond the ninth adsorption step at $k_{(14,8)}$, in contrast to the (13, m) complexes, which adsorb up to $k_{(13,11)}$, $m_{max} = 12$.
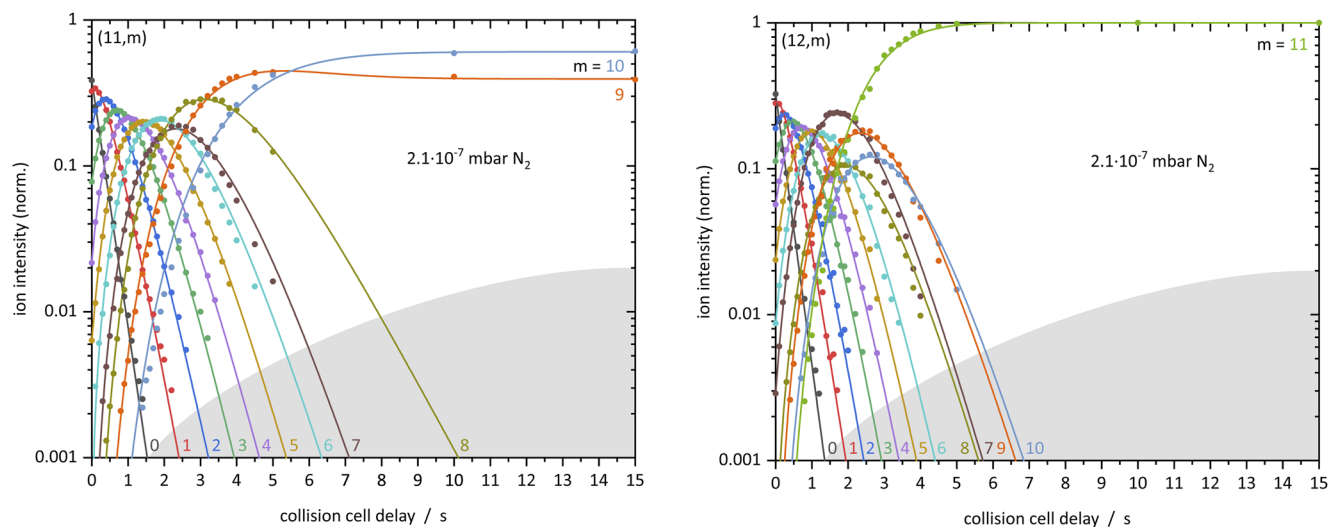

FIG. 6. Isothermal kinetics of the stepwise N_2 adsorption by isolated Fe_{11}^+ (left) and Fe_{12}^+ (right) clusters within 4.0×10^{-6} mbar He buffer gas and 2.1×10^{-7} mbar of N_2 (solid dots) at 26 K. The pseudo-first-order kinetic fits (solid lines) reveal reaction chains of up to 11 consecutive steps.
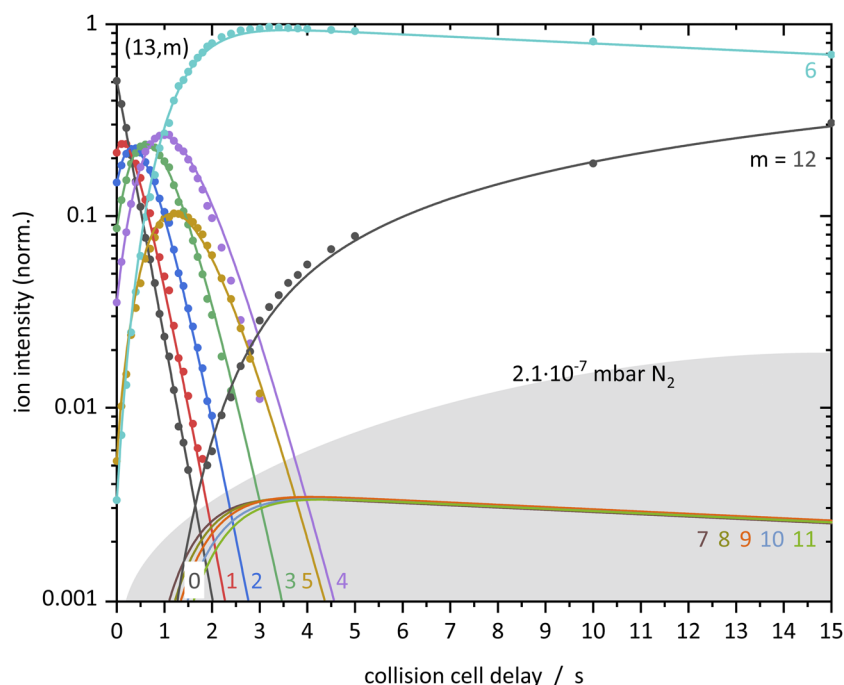
FIG. 7. Isothermal kinetics of the stepwise N_2 adsorption by the isolated Fe_{13}^+ cluster within 4.0×10^{-6} mbar He buffer gas and 2.1×10^{-7} mbar of N_2 (solid dots) at 26 K. The pseudo-first-order kinetic fits (solid lines) reveal reaction chains of up to 12 consecutive steps. We do not detect cluster adsorbate complexes m = 7–11. Modeling assumes that their intensities lie below our experimental noise level although some experiments did observe low levels of these species.

For Fe_n clusters with $n > 13$, there are just a few published DFT studies. The predicted most stable structures for neutral and cationic $Fe_{14}^{0/+}$ is the transformation from the icosahedron to a bicapped hexagonal antiprism.[60,61,100] The $n = 13$ to $n = 14$ transition is of particular interest. Predictions are that the extra adatom integrates at a bridging μ_2 position that may relax into a hexagonal ring upon further addition of adatoms.

There are similar N_2 uptake kinetics for clusters $n = 15$ and 16 (Fig. 9). Both reveal a most intense cluster adsorbate complex at $(n, m_{max-2}) = (15, 5)$ and a metastable adsorption
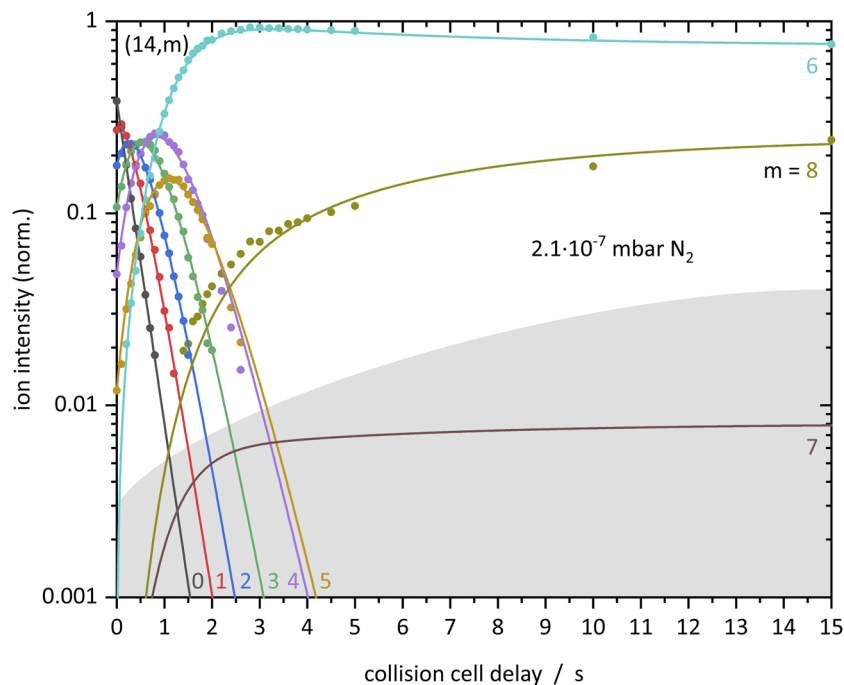

FIG. 8. Isothermal kinetics of the stepwise N_2 adsorption by the isolated Fe_{14}^+ cluster within 4.0×10^{-6} mbar He buffer gas and 2.1×10^{-7} mbar of N_2 (solid dots) at 26 K. The pseudo-first-order kinetic fits (solid lines) reveal N_2 uptake in up to eight consecutive steps and competing losses in the final two steps. Note the striking difference to the $n = 13$ case.
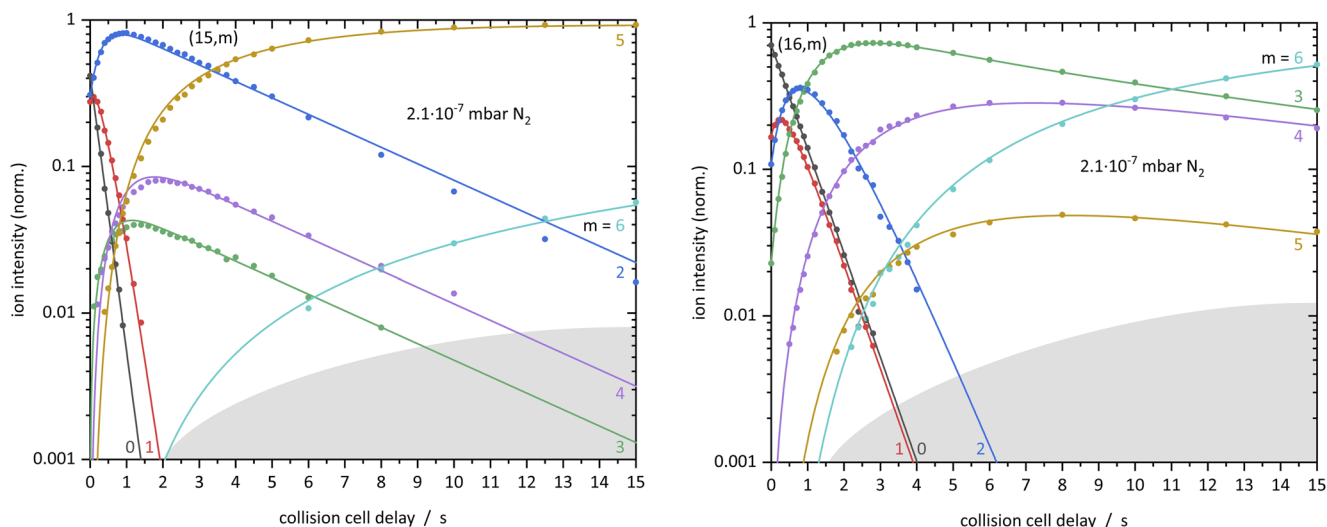
FIG. 9. Isothermal kinetics of the stepwise N_2 adsorption by the isolated Fe_{15}^+ (left) and Fe_{16}^+ (right) clusters within 4.0×10^{-6} mbar He buffer gas and 2.1×10^{-7} mbar of N_2 (solid dots) at 26 K. The pseudo-first-order kinetic fits (solid lines) reveal reaction chains of up to six consecutive steps in partial completion with desorption.

limit at $(n, m_{max-5}) = (15, 2)$. We note in passing that the Fe_{15}^+ cluster is more reluctant to take up N_2 under present conditions than any other cluster examined. This is documented by the observed saturation stoichiometry, $m_{max}/n = 0.47$, less than a one-to-two ratio, which is far away from a Langmuir type one-to-one behavior. It is another peculiar finding that both clusters, $n = 15$

and 16, experience considerable N_2 desorption at medium levels of coverage (cf. Figs. S41 and S42 and Tables S22 and S23).

All of the predicted most stable structures for neutral and cationic $Fe_{15}^{0/+}$ are bicapped hexagonal antiprisms.[24,58,60,61,64,100] Both six membered-rings of the hexagonal antiprism are capped with a single Fe atom, and there is a single Fe atom in the center. The
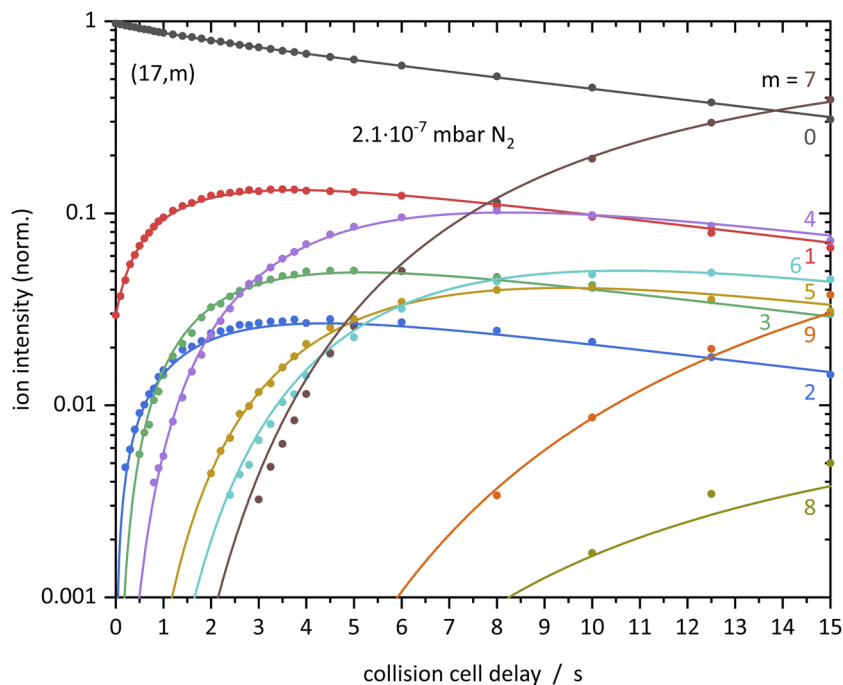

FIG. 10. Isothermal kinetics of the stepwise N_2 adsorption by the isolated Fe_{17}^+ cluster within 4.0×10^{-6} mbar He buffer gas and 2.1×10^{-7} mbar of N_2 (solid dots) at 26 K. The pseudo-first-order kinetic fits (solid lines) reveal reaction chains of up to nine consecutive steps.

neutral and cationic $Fe_{16}^{0/+}$ clusters are said to follow a "hexagonal-antiprism packing," in which the extra Fe adatoms join on one of the two capped hexagons.[60,61,100] The next neighbor coordination numbers of such a cluster geometry do not allow us to draw kinetic conclusions that would point toward our experimental observations. Further factors beyond the structures seem at play.

a. The special n = *17 case.* Some of our early and preliminary experiments had revealed an absolute reluctance against N_2 uptake by the Fe_{17}^{+} clusters. This finding had been reproducible throughout repetitive runs of experiments. By careful tuning of experimental conditions—in particular, minute adjustments of trapping and transfer potentials—we managed to observe some $[Fe_{17}(N_2)_m]^{+}$ complexes. Note that clusters of other sizes did not change their behavior in a noticeable way upon comparable adjustments. From this observation, we conclude there is very facile desorption in the case of $n = 17$.

Under the most "gentle" conditions achievable, we observe a significantly slower but noticeable N_2 adsorption to Fe_{17}^{+} compared to all other clusters (Fig. 10). Note that 30% of the initially bare Fe_{17}^{+} clusters remain naked even after storing them for 15 s in the presence of the N_2 environment and thermalizing He buffer gas within the RF hexapole trap. By inspection of the fitted rate constants, it becomes apparent that the desorption rate constants $k_{-(17,1)}$ and $k_{-(17,2)}$ are larger than the corresponding adsorption rate constants $k_{(17,0)}$ and $k_{(17,1)}$ (cf. Fig. S43 and Table S24). The resulting balance seems responsible for the delicate response to experimental conditions. Further desorption rate constants $k_{-(17,m)}$ are of significance in our fits for almost all steps m. This and the subsequent $n = 18$ case discussed below are the only clusters where there is appreciable N_2 desorption at all values of m.

In the case of $n = 17$, we undertook another set of kinetic investigations at elevated pressures of N_2 (4.7×10^{-7} mbar N_2) with identical conditions otherwise (Fig. S19). The N_2 uptake remains slow, but some of the N_2 desorption steps become significantly slower (Fig. S44 and Table S25). Therefore, the rapid N_2 desorption—special to $n = 17$—appears to be quenched by N_2 collisions.

There are a few DFT predictions of $Fe_{17}^{0/+}$ cluster structures that find capped hexagon antiprisms for the neutral and cationic cases.[60,61,100] The capping iron atoms are all on the same side of the hexagonal antiprism, and they gather in a triangle on this side of the cluster. It is not obvious how such a cluster geometry enables the observed special kinetic features.

Summarizing our kinetic findings in this $m_{max} = n - 8$ region, we do not find an obvious correspondence with the DFT predictions on cluster structures. It seems inevitable to interpret the kinetic findings in light of additional influential factors, such as the electronic structure and how it might change upon N_2 adsorption.

In this context, we envision the following three working hypotheses for the $m_{max} = n - 8$ behavior of Fe_{14-17}^{+}:

(1)   The N_2 adsorbate reorganization might be hindered. The first N_2 molecules adsorb μ_1 end-on to the cluster complex with a slightly tilted motif over an edge or face. Subsequent to the adsorption of $n - 8$ N_2 molecules, a reorganization is needed to adsorb more N_2. Compared to the Fe_{13}^{+} case where an adsorbate reorganization must take place after the metastable

adsorption limit, a reorganization is not possible for these bigger cluster adsorbate complexes.

(2)   The Fe_{14-17}^{+} cluster might possess capped hexagonal antiprism geometry, which would accept less N_2 adsorbates. The enthalpic arguments for such behavior—as opposed to largely icosahedral structural motifs otherwise—need to be elucidated by dedicated modeling beyond the present exploratory studies in the future.

(3)   If there is a connection between enhanced N_2 uptake and high-spin relaxation—as discussed further in the following and the adjoining [IRS]—then the hexagonal antiprismatic Fe_{14-17}^{+} clusters may experience local spin pinning at some of their surface atoms, which would hinder stoichiometric N_2 uptake.

Orbital occupations of these clusters might be such that seven out of $n - 1$ surface atoms refuse to accept electron density from the N_2 lone-pair donor orbital, thus rendering their attachment unlikely. In contrast, the remaining Fe surface atoms readily do so. Thus, we speculate that there are two kinds of surface atoms in the Fe_{14-17}^{+} cluster range.

4. Fe_{18}^{+} – Fe_{20}^{+}—the m_{max} = n – 2 behavior indicates a second interior atom

We find that the $n = 18$–20 clusters adsorb N_2 readily up to an $m_{max} = n - 2$ limit. These three clusters also reveal metastable adsorption limits that are larger than those of the $n = 15$–17 clusters. Up to these metastable limits of (18, 7), (19, 9), and (20, 11), the stepwise N_2 uptake points toward "*smooth* surface" behavior. Beyond this limit, the N_2 uptake becomes irregular and thus specific to the occupied adsorption sites—a "*rough* surface" behavior. Despite these analogies, the adsorption kinetic of Fe_{18}^{+} is completely different compared to the adsorption kinetics of Fe_{19}^{+} and Fe_{20}^{+}.

a. The very special case of Fe_{18}^{+}. The kinetics of N_2 uptake by Fe_{18}^{+}, the (18, m) case, is the prominent instance of very involved adsorption behavior. The semi-logarithmic plot of the parent intensity Fe_{18}^{+} upon N_2 uptake reveals a short-term steep decrease, an intermediate plateau, and a slow decline past 3.6 s reaction delay (Fig. 11 and emphasized in Fig. S22). Note that we have reproduced this behavior multiple times and under minute variations of reaction conditions (pressure, temperature, ion optics potentials, and ion source conditions). The behavior is completely reproducible. Figure S21 documents a nominal "best fit" of the recorded kinetic curves when assuming ordinary stepwise single N_2 adsorption and desorption only. Such a fit obviously fails.

The assumption of a mix of at least two isomers is strongly supported by the clear observation of the almost constant plateau of Fe_{18}^{+} intensities at medium reaction delays (t = 1–3 s). It finds further support from the fact that N_2 reactant pressure variation does NOT change the relative intensity of this plateau. It thus stems from processes in the context of ion generation within the cluster ion source, namely, isomerism.

Two DFT studies of neutral and cationic $Fe_n^{0/+}$ clusters have predicted a "hexagonal-antiprism packing" for $Fe_{18}^{0/+}$.[61,100] This implies a square cap on one side of the antiprism. Unfortunately, such structures do not lend obvious support to the kinetic N_2 adsorption maximum $m_{max} = n - 2$ nor to the elucidated coexistence
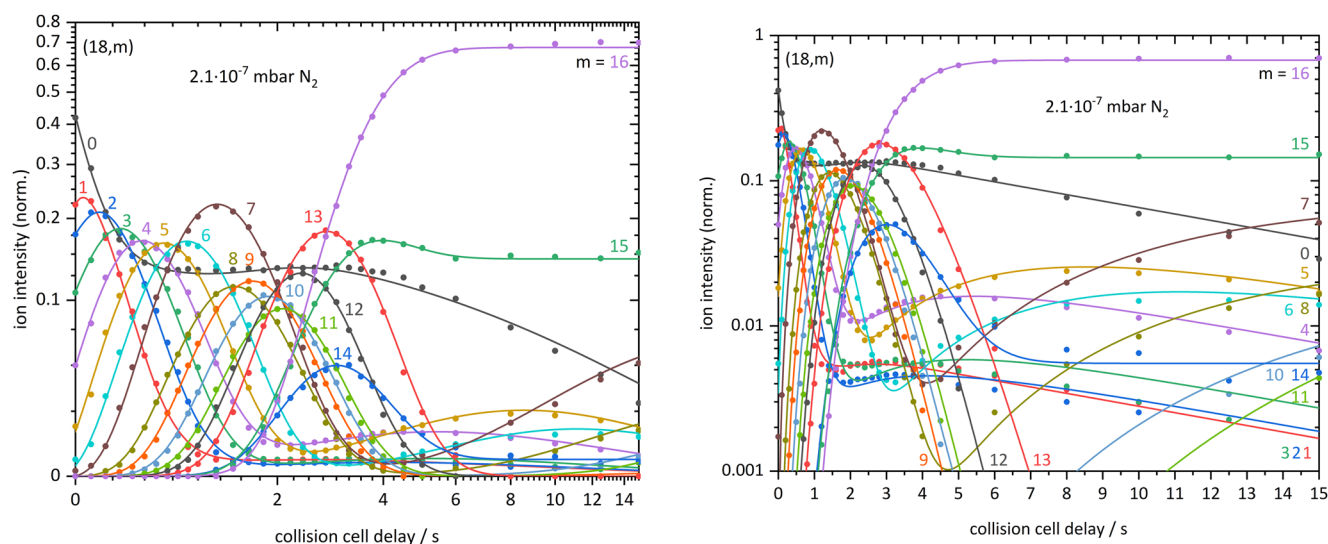
FIG. 11. Isothermal kinetics of the stepwise N_2 adsorption by the isolated Fe_{18}^+ cluster within 4.0×10^{-6} mbar He buffer gas and 2.1×10^{-7} mbar N_2 (solid dots) at 26 K. The pseudo-first-order kinetic fits (solid lines) reveal reaction chains up to 16 consecutive steps. Each fitting line comprises a sum of contributions from two isomer species, **A** and **B** (see text). This fit represents the minimum conversion scenario (MIC) between these two isomers. Note the different axis scaling: equidistant data points by nonlinear data transformation (left) and semi-logarithmic (right). A more detailed view of the initial area (0–4 s) can be found in Fig. S24. The corresponding fit of maximum conversion scenario (MAC) can be found in the supplementary material. See the text for the definition of MIC and MAC scenarios.

of isomers **A** and **B**. A double icosahedral structure "minus one" of Fe_{18}^+, similar to the predicted one of Fe_{19}^+,[24,58,59,61] would provide for two Fe atoms inside an outer, largely *smooth* Fe shell. This would provide a feasible explanation for our observed adsorption maximum $m_{max} = n - 2$ (Fig. 2).

Our own DFT endeavors revealed conceivable candidate structures of Fe_{18}^+, which are discussed at length, in the accompanying [IRS] paper. Note that these calculations are exploratory and meant to prepare for more definitive studies in the future. It seems as if a largely icosahedral motif (**18ico**) might compete with a hexagonal antiprismatic motif (**18hex**). The cubic closely packed motif (**18cp**) seems less stable by more than 200 kJ/mol (Fig. 12). Most importantly, all of these motifs seem to comprise comparable high-spin states, multiplicities of M = 56 and 58. Thus, the exploratory DFT
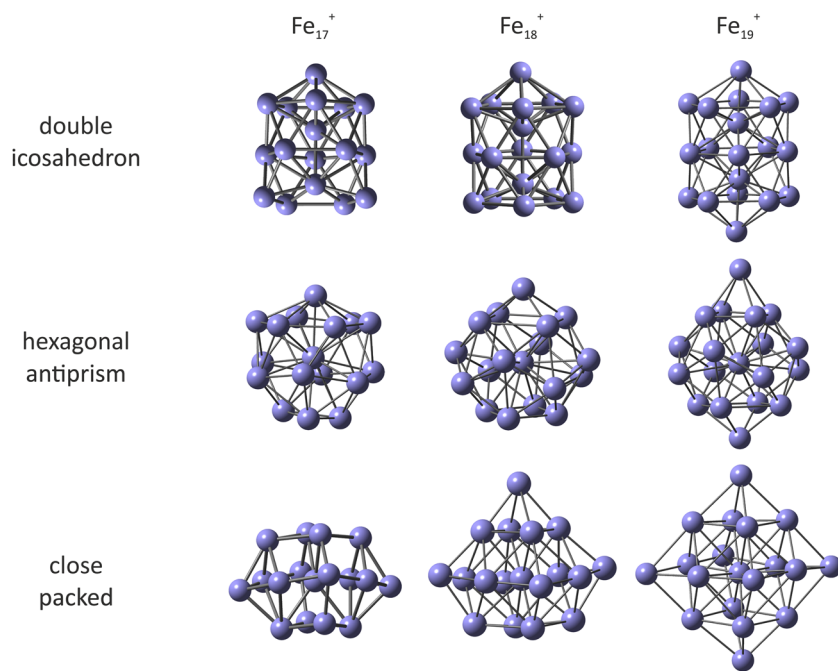

FIG. 12. Some DFT predicted geometries of Fe_{17}^+ (left), Fe_{18}^+ (center), and Fe_{19}^+ (right).

results point toward a purely geometric isomerism rather than to the coexistence of mere spin isomers. Note that the published XMCD studies conclude that there are high magnetic moments of almost constant 3.2–3.9 μ_B/Fe atom throughout the size range of Fe_n^+ clusters, n = 3–20, which agrees perfectly with our exploratory DFT studies.[14,46]

Because of the intrinsic complexity of the given task, our own DFT studies were conducted at the Perdew–Burke–Ernzerhof (PBE) level of theory without admixture of Hartree Fock exchange. In particular, our available computing resources did not allow for an equivalent survey at the enhanced level of hybrid exchange correlation functionals such as PBE0 or TPSSh. In this regard, we take the absolute values of computed stabilities with a grain of salt. In particular, two of the predicted isomers of Fe_{18}^+ come with comparable stabilities, and we take this as a qualitative finding. Beyond this, our computations do not allow for a quantitative prediction of energetic differences between the icosahedral motif (**18ico**) and the hexagonal antiprismatic motif (**18hex**). Moreover, it seems reasonable to rely on the prediction of lesser stability of the close packed motif (**18cp**) (Fig. 12).

Returning to the discussion of the recorded kinetics in terms of two (possibly three) participating isomers of Fe_{18}^+, we need to find answers to at least three questions:

(a) Is it possible to obtain a unique fit of the coupled N_2 adsorption dynamics of both isomers?
(b) Does the second isomer originate exclusively from the cluster source, or is some interconversion by the stepwise N_2 adsorption conceivable?
(c) If interconversion of isomers occurs by N_2 adsorptions, does it occur upon low or high or any N_2 coverages?

After an extended survey of conceivable fitting schemes and after invoking at least three different fitting programs to model five independent kinetic datasets, the answer to question (a) is

negative. Ambiguities remain whatever approach is taken. Nevertheless, it became possible to extract significant findings from our concerted fitting attempts.

In particular, we found it possible to achieve kinetic fits of high quality (cf. Figs. S24, S26, and S30) for three limiting cases, which we label as *minimum conversion* (MIC), *maximum conversion* (MAC), and *delayed activation conversion* (DAC) scenarios. Of course, other conversion levels are conceivable, in particular, those that fall in between MIC and MAC. The highly speculative DAC scenario is elaborated in the supplementary material (cf. Text 6/Figs. S30–S33/Tables S10–S14) and does not yield further insight but shares the main finding with MIC and MAC, as discussed below. The MIC scenario implies coupling of as little isomeric adsorbate species as possible, and MAC implies coupling of as many such species as possible. Note that MIC sees complete N_2 desorption, whereas MAC sees some incomplete N_2 evaporation (cf. blue and red curves in Fig. 13).

Addressing question (b), we state that there is a likely admixture of about 10% up to at most 13% of a minor isomer of Fe_{18}^+ originating from the cluster ion source. Note that there is no such evidence for any other cluster size. We label the initially major isomer of Fe_{18}^+, $I_o \approx 0.42$, as $^A Fe_{18}^+$ and the minor isomer of Fe_{18}^+, $I_o \approx 0.10$, as $^B Fe_{18}^+$. The remaining initial intensities (I_o = 0.48) are distributed among products with few N_2 adsorbates [see the supplementary material for further discussion of the procedure of ion admission to the hexapole trap and on starting points for kinetic recording and fitting procedures (cf. ESI Text 3.1)].

In order to address question (c), we examine the measured rate constants for adsorption and desorption of N_2 to and from Fe_{18}^+ as differentiated for isomers **A** and **B** and for the two limiting conversion cases, MIC and MAC (Figs. S25 and S27).

The N_2 uptake of isomer **A** is independent of the assumed conversion scheme. MIC and MAC scenarios yield identical rate
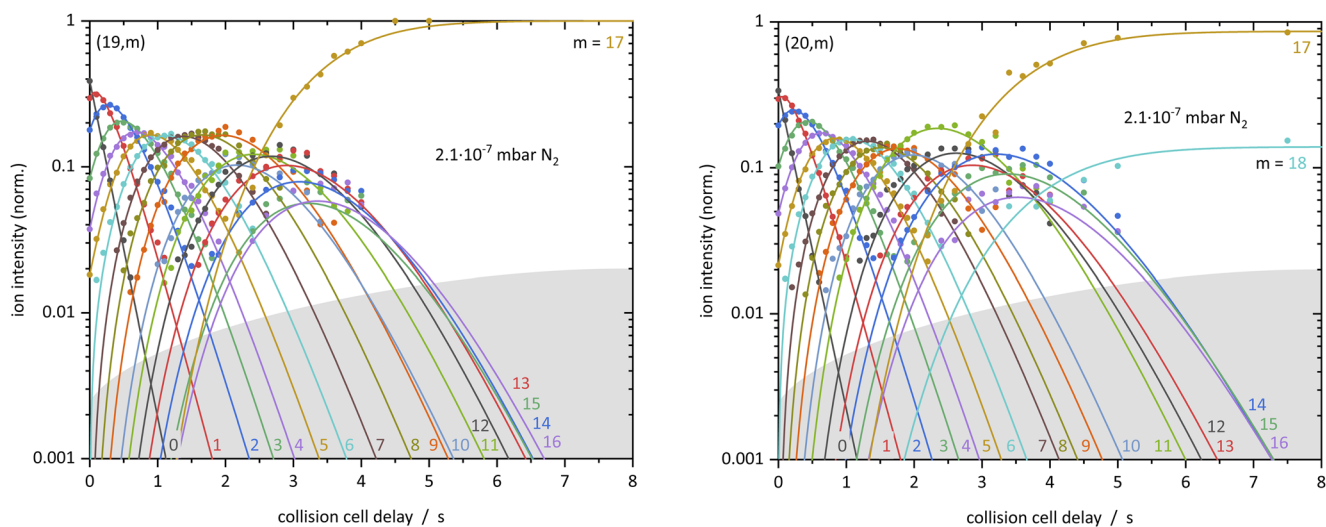
FIG. 13. Conversion rates of isomer **A** (loaded with m_A N_2s) to isomer **B** (loaded with m_B N_2s) for the MIC (green) and MAC scenarios (black, blue, and red). Note the presence of m = 9 conversion step in both cases, which leads to complete expulsion of all N_2 adsorbates.

constants (cf. Figs. S25 and S27, black solid and open symbols). In particular, it is a robust finding that $^{A}Fe_{18}(N_2)_7^+$ and $^{A}Fe_{18}(N_2)_{13}^+$—the m = 7 and 13 cases of isomer **A**—experience a reduced N_2 uptake as evidenced by the according dips in the fitted rate constants and the concomitant enhancement of intermediate product intensities in the recorded kinetic curves. Desorption is exclusive to m > 13 and thus points to the occurrence of weakly bound N_2 adsorbates upon high levels of coverages by 15 and 16 N_2 molecules. The significantly enhanced adsorption rate constant at $^{A}k_{(18,14)}$ is evident in MIC, MAC, and DAC scenarios but is void of an obvious interpretation. It is highly speculative but conceivable to consider an adsorbate shell reorganization (all tilted N_2 to all end-on N_2 in favor of adsorbate shell closure).

The N_2 uptake of isomer **B** is significantly more complicated (cf. Figs. S25 and S27, red solid and open symbols). In the cases of MIC and MAC scenarios, the first adsorption step $^{B}k_{(18,0)}$ = 0.1 s^{-1} is significantly slower than the following adsorption steps. We see strong variations in adsorption and desorption rate constants. For both scenarios, the tenth adsorption step $^{B}k_{(18,9)}$ is fast, as are the m = 1–3 adsorption steps. In both scenarios, several desorption rates constants are larger than the corresponding adsorption rate constants, e.g., $^{B}k_{-(18,8)}$ > $^{B}k_{(18,7)}$ for the m = 7 step. That leads to a strong slowdown within the chain of consecutive adsorptions. It is common to the MIC and MAC scenarios that there are high levels of adsorption and desorption that are modulated strongly by the adsorbate level m. MIC stops at m = 10, whereas MAC reveals significant rate constants up to m = 15.

Most importantly, the conversion rate constants, which turn isomer **A** into isomer **B** (Fig. 13), are significant at or around m = 9 and include a concomitant expulsion of all of the accumulated N_2 adsorbates. This holds for both MIC and MAC scenarios. Such an expulsion would be highly endothermic, estimated as almost 300 kJ/mol by our exploratory DFT calculations. A driving force for such expulsion would need to originate from another coupled process. Candidate processes are (a) geometric relaxation, (b) spin conversion, and (c) N_2 activation and any combination of these. Process (c) is in contradiction to the observation of complete N_2 expulsion—none of the adsorbed N_2 molecules is left behind upon isomeric conversion. Process (b) is not supported by our exploratory DFT modeling, i.e., spin relaxation seems stepwise, small and does not provide significant enthalpic gains. Finally, process (a) would need to be dramatic and much beyond the nearly isoenergetic candidate structures **18ico** and **18hex**, where the two most likely forms are almost degenerate (irrespective of spin state). Thus, the large driving force suggests consideration of the third conceivable isomer **18cp** because it qualitatively provides about 200 kJ/mol of excess enthalpy. In this regard, our exploratory DFT modeling does provide for some guidance toward an enthalpic interpretation of the kinetic findings. Upon uptake of seven or more N_2 adsorbates, the **18cp** structure might relax to **18ico** and/or **18hex,** while the excess relaxation enthalpy serves to evaporate all of the N_2 adsorbates.

Summarizing our present understanding of the prevailing N_2 adsorption kinetics of Fe_{18}^+, we have depicted a generalized scheme of isomeric Fe_{18}^+ conversion through stepwise N_2 adsorption (Fig. S23). This scheme emphasizes the MIC scenario with complete adsorbate expulsion but interpolates somewhat toward the MAC scenario with some N_2 adsorbates remaining upon isomer conversion. The temporal evolution of isomers **A** and **B** in total and per species is provided elsewhere (Figs. S28 and S29).
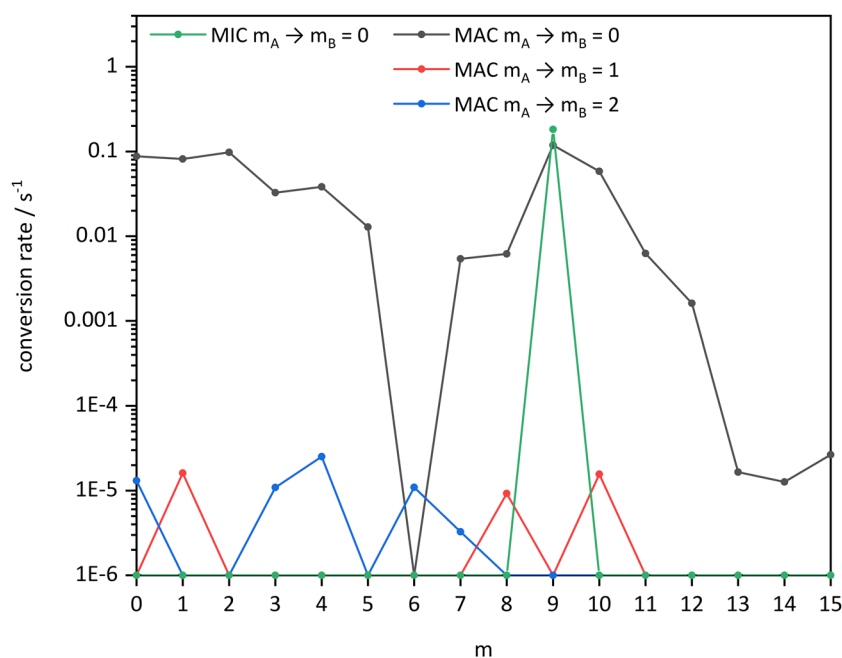
FIG. 14. Isothermal kinetics of the stepwise N_2 adsorption by isolated Fe_{19}^+ (left) and Fe_{20}^+ (right) clusters within 4.0×10^{-6} mbar He buffer gas and 2.1×10^{-7} mbar of N_2 (solid dots) at 26 K. The pseudo-first-order kinetic fits (solid lines) reveal reaction chains of up to 18 consecutive steps in a likely *smooth* surface adsorption fashion.

Beyond our tentative interpretation of the kinetic data and their fits, there is one robust finding from the MIC, MAC, and DAC fits. There must be an initial mixture of at least two isomers of naked Fe_{18}^+ generated in the cluster ion source. There is no evidence for more than one isomer in any other investigated case of Fe_n^+ ($n \neq 18$).

On the basis of insights gained from the adsorption kinetics and modeling, from our exploratory DFT studies and from published DFT studies by others, we now attempt to relate the isomers **A** and **B** to the calculated isomeric structures, **18ico**, **18hex**, and **18cp**. By enthalpic arguments, we find it necessary to relate major isomer **A** to **18cp**, as evidenced above. This leaves minor isomer **B** to interpret. Some guidance comes from the recorded adsorption limits (Fig. 2), which reveal values $m_{max} = n - 8$ in the range of $n > 13$, while $m_{max} = n - 1$ and $n - 2$ are observed at $n = 13$ and $n = 19$, respectively. Thus, Fe_{13}^+ and Fe_{19}^+ likely possess icosahedral structures. In line with this, we conclude that the minor isomer $^B Fe_{18}^+$ might coincide with some largely icosahedral structure close to the calculated isomer **18ico**, with small contributions of **18hex** possible. It is conceivable that smaller Fe_n^+ clusters that show "$n - 8$" maximum absorption assume hexagonal structural motifs. We take these assignments as our working hypothesis from here on.

b. Fe_{19}^+ *and* Fe_{20}^+. It is much simpler to interpret the recorded N_2 adsorption kinetics of (19, m) and (20, m) (Fig. 14). We have observed adsorption limits m_{max} at (19, 17) and (20, 18) and metastable adsorption limits m_x at (19, 9) and (20, 11), and there is a most intense cluster adsorbate complex m^* at (20, 17).

Both clusters $n = 19$ and 20 undergo swift N_2 adsorption in a stepwise fashion at equal pace (cf. Figs. S45 and S46 and Tables S26 and S27). This indicates *smooth* surface behavior of equivalent adsorption sites. The genetic fitting algorithm insists on some contributions of slow N_2 desorption at $k_{-(20,8)}$, $k_{-(20,14)}$, and $k_{-(20,15)}$. These are of little significance in the overall kinetics. Past the metastable adsorption limit, the quality of fits diminishes. We attribute this effect to the transition from *smooth* to partially *rough* surface behavior at this point. *Rough* surfaces may experience parallel N_2 adsorption to distinguishable surface sites, which inherently presents difficulties in modeling by simple stepwise kinetics. In contrast, the last desorption step at $k_{-(20,18)}$ is significant. It leads to an N_2 adsorption/desorption equilibrium, which indicates that the 18th N_2
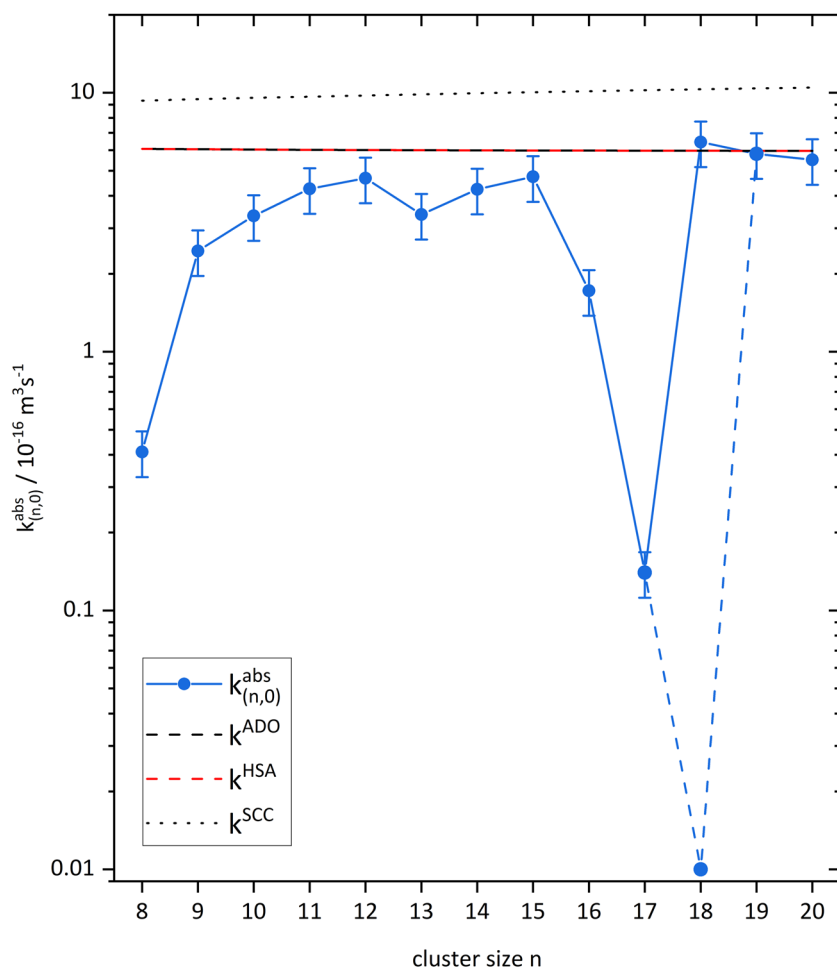

FIG. 15. Absolute rate constant $k_{(n,0)}^{abs}$ of the initial N_2 adsorption to Fe_n^+ clusters by experiment (blue dots, estimated error bars), according to classical average dipole orientation (ADO) theory (black dashed line), to the hard-sphere average (HSA) dipole orientation model (red dashed line), and to the surface charge capture model (dotted line). Note that the dashed blue line corresponds to the second unreactive Fe_{18}^+ isomer **B**. Also note that 10^{-16} m^3 s^{-1} = 10^{-10} cm^3 s^{-1}. Numerical values are listed in Table II.

TABLE II. Relative experimental and derived absolute N_2 adsorption rate constants for the initial N_2 adsorption to Fe_n^+ clusters in comparison to the calculated rate constants by classical ADO theory, the HSA model, and the SCC model. The experimental values, recorded at 4.0×10^{-6} mbar He buffer gas and 2.1×10^{-7} mbar of N_2 within the RF hexapole trap at 26 K, bear an estimated uncertainty of $\pm 20\%$. Note that 10^{-16} m^3 s^{-1} = 10^{-10} cm^3 s^{-1}.

n	$k_{(n,0)}$ (s^{-1})	$k_{(n,0)}^{abs}$ (10^{-16} m^3 s^{-1})	$k_{(n,0)}^{ADO}$ (10^{-16} m^3 s^{-1})	$k_{(n,0)}^{HSA}$ (10^{-16} m^3 s^{-1})	$k_{(n,0)}^{SCC}$ (10^{-16} m^3 s^{-1})
8	0.38	0.41	6.07	6.07	9.33
9	2.2	2.45	6.05	6.05	9.44
10	3.1	3.35	6.03	6.03	9.55
11	3.9	4.26	6.02	6.02	9.66
12	4.3	4.68	6.01	6.01	9.76
13	3.1	3.39	6.00	6.00	9.86
14	3.9	4.24	5.99	5.99	9.96
15	4.3	4.74	5.99	5.99	10.05
16	1.6	1.72	5.98	5.98	10.14
17	0.13	0.14	5.98	5.98	10.23
18 **A**	5.9	6.45	5.97	5.97	10.32
18 **B**	0.01	0.01	5.97	5.97	10.32
19	5.3	5.81	5.97	5.97	10.40
20	5.0	0.55	5.96	5.96	10.48

adsorbate is loosely bound and (20,17) might correspond to a first adsorbate shell closure.

DFT modeling finds two conceivable structures for m = 19. First, there is a double icosahedron as determined mainly for the cationic Fe_{19}^+ cluster.[24,58,59,61] Second, there is a capped hexagonal antiprism for the neutral Fe_{19} cluster.[24,59,61,101] This hexagonal antiprism is capped on one side with a square pyramid. For the neutral and cationic $Fe_{20}^{0/+}$, modeling predicts a double icosahedron that is capped on one side with a Fe atom.[24,59,61] The double icosahedron structure of Fe_{19}^+ would explain the $m_{max} = n - 2$ adsorption limit by its two inaccessible, inner atoms. Moreover, there is a conceivable interpretation of the metastable adsorption limit m_x at (20, 11) by adding the eleven N_2 to the one four-fold and ten sixfold coordinated Fe atoms. Up to the adsorption limit m_{max} at (20, 18), seven more N_2 molecules can add to the two sevenfold, three eightfold, and two ninefold coordinated Fe atoms.

5. Absolute rate constants of the initial N_2 adsorption

The absolute rate constants $k_{(n,m)}^{abs}$ were derived from the pseudo-first-order relative rate constants by normalization to the local N_2 reactant number density. We obtain such values for the initial uptake of the first N_2 adsorbate as a function of cluster size (Fig. 15, blue dots). Note that there are small uncertainties among the rate constants as a function of cluster size n, may be better than $\pm 5\%$, whereas all of the absolute values bear an estimated uncertainty of $\pm 20\%$.

For comparison, we calculated the collision rate constants according to the classical ADO theory, the HSA, and the SCC models (Table II). Within the given experimental uncertainties, the highest values of recorded rate constants agree favorably with the theoretical predictions. The small Fe_n^+ clusters n = 8–10 are somewhat reluctant to adsorb N_2, which relates to limited heat baths (fewer vibrational degrees of freedom) for dissipation of the heat of N_2 adsorption. The Fe_{13}^+ cluster reveals a small dip in N_2 adsorption rate constants that seemingly relates to its all *smooth* surface.

Most prominently, there is the remarkable dip toward reluctance of N_2 interaction at Fe_{17}^+, and even more so at the **B** isomer of Fe_{18}^+. The structural and/or electronic implications are unknown as of now and await high-level quantum chemical modeling much beyond our own exploratory low-level attempts.

IV. CONCLUSIONS

We present a study of stepwise N_2 adsorption on size-selected Fe_n^+ (n = 8–20) clusters. We have recorded their adsorption kinetics at 26 K in a hexapole collision cell and performed pseudo-first-order kinetic fits, which show stepwise N_2 adsorption. The N_2 uptake reaches an adsorption limit (m_{max}) with $m_{max} : n \leq 1$ in all investigated cases. In some cases, the adsorption limit m_{max} is not the most intense cluster adsorbate complex. This feature varies with cluster size.

We are able to identify four characteristic regions of (n, m_{max}) stoichiometries: Small clusters, n = 7, 8, reveal $m_{max} = n$, with a "surface only" type structure. The smaller medium-sized clusters, n = 9–13, reveal $m_{max} = n - 1$, with likely icosahedral structural motifs with a single inner Fe atom that is not accessible for N_2 adsorption. In particular, the Fe_{13}^+ cluster very likely assumes a highly symmetric icosahedral structure. The larger medium-sized clusters, n = 14–17, reveal an adsorption behavior of $m_{max} \approx n - 8$, and they likely assume "hexagonal antiprismatic" structural motifs. The large clusters, n = 18–20, reveal $m_{max} = n - 2$ adsorption limits that point toward capped icosahedral structures comprising two inner atoms. The Fe_{19}^+ cluster can be envisaged as a highly symmetric bi-icosahedron.

We find a strong temperature dependence of N_2 adsorption in the range of T = 21–28 K, and we identify two regions of low and

high adsorption loads above and below 24 K, respectively. The Fe_{17}^+ cluster shows the largest temperature dependence with N_2 adsorption vanishing at 22 K, which marks a remarkable case of nitrogen phobia that is unprecedented.

Our recorded adsorption kinetics reveals three cases with an especially conspicuous adsorption behavior. First, there is the Fe_{13}^+ cluster, which pauses at its metastable adsorption limit m = 6 but proceeds very rapidly by further stepwise adsorption up to $m_{max} = 12$. We speculate that there is a highly symmetric $Fe_{13}(N_2)_6^+$ complex with a maximum amount of $Fe-N_2$-interaction hindering the seventh and further N_2 uptakes.

Second, there are the Fe_{17}^+ kinetics, located in the particularly noteworthy medium size region of n = 14–17 with adsorption limits $m_{max} = n - 8$. Fe_{17}^+ has the slowest initial N_2 uptake among all recorded clusters. Our kinetic analysis points toward significant or even high kinetic rates of N_2 desorption in competition to the N_2 adsorption such that the net uptake becomes slow. We have not yet achieved a conclusive interpretation of the high desorption rates that occur for Fe_{17}^+ as opposed to all other clusters.

Third, there is the very special case of Fe_{18}^+, which reveals the only N_2 uptake kinetics with a bi-exponential decay for the bare cluster ion, providing strong evidence for isomeric mixtures. By application of several conceivable fitting schemes, we identify three limiting cases of *minimum conversion* (MIC), *maximum conversion* (MAC), and *delayed activation conversion* (DAC), all of which unequivocally support the two-isomer hypothesis and which necessarily invoke the conversion of a major isomer into a minor one upon uptake of some 8 or 9 N_2 adsorbate molecules. With the help of our own exploratory DFT studies, we tentatively identify candidate structures for these isomers, namely, closely packed structure **18cp** as the major isomer **A**, which relax into the more favorable icosahedral/hexagonal antiprismatic structure **18ico/hex** by expulsion of the adsorbed N_2 layer.

In all of these cases, the net positive charge of the iron clusters enhances binding by charge-induced dipole interactions but also hampers π backdonation. These and other effects provide a subtle balance that might modulate under the influence of a net charge and of cluster geometry.[100,101] We are investigating such charge effects by further experiments on anionic clusters, which will be reported in due time.

SUPPLEMENTARY MATERIAL

See the supplementary material for further adsorption limits; temperature dependent limits for different N_2 pressures; tabulated values for the rate constants, collision rates, and sticking probability; and the three different fitting possibilities (MIC, MAC, and DAC) with their unique characteristics.

ACKNOWLEDGMENTS

AUTHOR DECLARATIONS

Conflict of Interest

The authors have no conflicts to disclose.

Author Contributions

A.S., M.P.K., D.V.F., M.E.H., J.M., S.D., and G.N.-S. conducted the experiments. A.S. and C.W. conducted the quantum chemical calculations. A.S., D.S., and G.N.-S. conducted the kinetic fits algorithms. A.S., P.B.A., and G.N.-S. evaluated all data and wrote the manuscript, which all authors agreed to.

DATA AVAILABILITY

The data that support the findings of this study are available from the corresponding author upon reasonable request.

REFERENCES

[1] P. Boissel, Astron. Astrophys. **285**, L33 (1994).

[2] D. K. Böhme and H. Schwarz, Angew. Chem., Int. Ed. Engl. **44**, 2336 (2005).

[3] G. J. Kubas, Chem. Rev. **107**, 4152 (2007).

[4] P. B. Armentrout, Catal. Sci. Technol. **4**, 2741 (2014).

[5] N. Russo and D. R. Salahub, *Metal-Ligand Interactions: Structure and Reactivity* (Springer Science & Business Media, 2012), Vol. 474.

[6] R. A. J. O'Hair, Chem. Commun. **2006**, 1469.

[7] M. D. Morse, M. E. Geusic, J. R. Heath, and R. E. Smalley, J. Chem. Phys. **83**, 2293 (1985).

[8] E. K. Parks, B. H. Weiller, P. S. Bechthold, W. F. Hoffman, G. C. Nieman, L. G. Pobo, and S. J. Riley, J. Chem. Phys. **88**, 1622 (1988).

[9] R. L. Whetten, D. M. Cox, D. J. Trevor, and A. Kaldor, Phys. Rev. Lett. **54**, 1494 (1985).

[10] M. D. Morse, Chem. Rev. **86**, 1049 (1986).

[11] M. M. Kappes, Chem. Rev. **88**, 369 (1988).

[12] L.-S. Wang, X. Li, and H.-F. Zhang, Chem. Phys. **262**, 53 (2000).

[13] P. Armentrout, Annu. Rev. Phys. Chem. **52**, 423 (2001).

[14] J. Meyer, M. Tombers, C. van Wüllen, G. Niedner-Schatteburg, W. Eberhardt, M. Neeb, S. Palutke, M. Martins, and W. Wurth, J. Chem. Phys. **143**, 104302 (2015).

[15] S. C. Richtsmeier, E. K. Parks, K. Liu, L. G. Pobo, and S. J. Riley, J. Chem. Phys. **82**, 3659 (1985).

[16] E. K. Parks, K. Liu, S. C. Richtsmeier, L. G. Pobo, and S. J. Riley, J. Chem. Phys. **82**, 5470 (1985).

[17] N. O. Jones, M. R. Beltran, S. N. Khanna, T. Baruah, and M. R. Pederson, Phys. Rev. B **70**, 165406 (2004).

[18] M. R. Zakin, R. O. Brickman, D. M. Cox, and A. Kaldor, J. Chem. Phys. **88**, 6605 (1988).

[19] J. Conceição, S. K. Loh, L. Lian, and P. B. Armentrout, J. Chem. Phys. **104**, 3976 (1996).

[20] L. Tan, F. Liu, and P. B. Armentrout, J. Chem. Phys. **124**, 084302 (2006).

[21] M. Li, S.-R. Liu, and P. B. Armentrout, J. Chem. Phys. **131**, 144310 (2009).

[22] J. B. Griffin and P. B. Armentrout, J. Chem. Phys. **106**, 4448 (1997).

29 April 2024 06:35:03

[23]C. P. McNary and P. B. Armentrout, Phys. Chem. Chem. Phys. **16**, 26467 (2014).

[24]A. Jedidi, A. Markovits, C. Minot, M. Abderrabba, and M. A. Van Hove, Phys. Chem. Chem. Phys. **16**, 20703 (2014).

[25]E. K. Parks, G. C. Nieman, L. G. Pobo, and S. J. Riley, J. Chem. Phys. **88**, 6260 (1988).

[26]M. P. Irion and P. Schnabel, J. Phys. Chem. **95**, 10596 (1991).

[27]K. O. Fossan and E. Uggerud, Dalton Trans. **2004**, 892.

[28]K. A. Jackson, M. Knickelbein, G. Koretsky, and S. Srinivas, Chem. Phys. **262**, 41 (2000).

[29]R. Liyanage, J. B. Griffin, and P. B. Armentrout, J. Chem. Phys. **119**, 8979 (2003).

[30]G. L. Gutsev, M. D. Mochena, and C. W. Bauschlicher, Chem. Phys. **314**, 291 (2005).

[31]B. H. Weiller, P. S. Bechthold, E. K. Parks, L. G. Pobo, and S. J. Riley, J. Chem. Phys. **91**, 4714 (1989).

[32]J. B. Griffin and P. B. Armentrout, J. Chem. Phys. **107**, 5345 (1997).

[33]M. Ichihashi, T. Hanmura, and T. Kondow, J. Chem. Phys. **125**, 133404 (2006).

[34]O. Gehret and M. P. Irion, Chem. Phys. Lett. **254**, 379 (1996).

[35]I. Valencia, Chem. Phys. **476**, 46 (2016).

[36]W. Zheng, S. N. Eustis, X. Li, J. M. Nilles, O. C. Thomas, K. H. Bowen, and A. K. Kandalam, Chem. Phys. Lett. **462**, 35 (2008).

[37]M. Sakurai, K. Watanabe, K. Sumiyama, and K. Suzuki, J. Chem. Phys. **111**, 235 (1999).

[38]W. D. Knight, K. Clemenger, W. A. de Heer, W. A. Saunders, M. Y. Chou, and M. L. Cohen, Phys. Rev. Lett. **52**, 2141 (1984).

[39]W. Miehle, O. Kandler, T. Leisner, and O. Echt, J. Chem. Phys. **91**, 5940 (1989).

[40]L. Lian, C. X. Su, and P. B. Armentrout, J. Chem. Phys. **97**, 4072 (1992).

[41]E. Kim, A. Mohrland, P. F. Weck, T. Pang, K. R. Czerwinski, and D. Tománek, Chem. Phys. Lett. **613**, 59 (2014).

[42]I. M. L. Billas, A. Châtelain, and W. A. de Heer, Science **265**, 1682 (1994).

[43]D. M. Cox, D. J. Trevor, R. L. Whetten, E. A. Rohlfing, and A. Kaldor, Phys. Rev. B **32**, 7290 (1985).

[44]W. A. de Heer, P. Milani, and A. Chatelain, Phys. Rev. Lett. **65**, 488 (1990).

[45]X. Xu, S. Yin, R. Moro, A. Liang, J. Bowlan, and W. A. de Heer, Phys. Rev. Lett. **107**, 057203 (2011).

[46]M. Niemeyer, K. Hirsch, V. Zamudio-Bayer, A. Langenberg, M. Vogel, M. Kossick, C. Ebrecht, K. Egashira, A. Terasaki, T. Moeller, B. V. Issendorff, and J. T. Lau, Phys. Rev. Lett. **108**, 057201 (2012).

[47]M. Wu, A. K. Kandalam, G. L. Gutsev, and P. Jena, Phys. Rev. B **86**, 174410 (2012).

[48]P. G. Alvarado-Leyva, F. Aguilera-Granja, L. C. Balbás, and A. Vega, Phys. Chem. Chem. Phys. **15**, 14458 (2013).

[49]D. E. Bergeron, A. W. Castleman, T. Morisato, and S. N. Khanna, Science **304**, 84 (2004).

[50]R. Burgert, H. Schnöckel, M. Olzmann, and K. H. Bowen, Jr., Angew. Chem., Int. Ed. Engl. **45**, 1476 (2006).

[51]G. L. Gutsev, M. D. Mochena, C. W. Bauschlicher, Jr., W.-J. Zheng, O. C. Thomas, and K. H. Bowen, J. Chem. Phys. **129**, 044310 (2008).

[52]Y. Jia and Z. Luo, Coord. Chem. Rev. **400**, 213053 (2019).

[53]P. Felício-Sousa, K. F. Andriani, and J. L. F. Da Silva, Phys. Chem. Chem. Phys. **23**, 8739 (2021).

[54]J. L. Chen, C. S. Wang, K. A. Jackson, and M. R. Pederson, Phys. Rev. B **44**, 6558 (1991).

[55]M. Castro and D. R. Salahub, Phys. Rev. B **49**, 11842 (1994).

[56]P. Ballone and R. O. Jones, Chem. Phys. Lett. **233**, 632 (1995).

[57]S. Yu, S. Chen, W. Zhang, L. Yu, and Y. Yin, Chem. Phys. Lett. **446**, 217 (2007).

[58]Q.-M. Ma, Z. Xie, J. Wang, Y. Liu, and Y.-C. Li, Solid State Commun. **142**, 114 (2007).

[59]G. L. Gutsev, C. A. Weatherford, P. Jena, E. Johnson, and B. R. Ramachandran, J. Phys. Chem. A **116**, 10218 (2012).

[60]O. Diéguez, M. Alemany, C. Rey, P. Ordejón, and L. Gallego, Phys. Rev. B **63**, 205407 (2001).

[61]H. K. Yuan, H. Chen, A. L. Kuang, C. L. Tian, and J. Z. Wang, J. Chem. Phys. **139**, 034314 (2013).

[62]T. Oda, A. Pasquarello, and R. Car, Phys. Rev. Lett. **80**, 3622 (1998).

[63]D. Hobbs, G. Kresse, and J. Hafner, Phys. Rev. B **62**, 11556 (2000).

[64]G. Rollmann, P. Entel, and S. Sahoo, Comput. Mater. Sci. **35**, 275 (2006).

[65]C. N. R. Rao and G. R. Rao, Surf. Sci. Rep. **13**, 223 (1991).

[66]E. D. Pillai, T. D. Jaeger, and M. A. Duncan, J. Phys. Chem. A **109**, 3521 (2005).

[67]S. Shetty, A. P. J. Jansen, and R. A. van Santen, J. Phys. Chem. C **112**, 17768 (2008).

[68]C. Kerpal, D. J. Harding, J. T. Lyon, G. Meijer, and A. Fielicke, J. Phys. Chem. C **117**, 12153 (2013).

[69]G. Ertl, Angew. Chem., Int. Ed. Engl. **47**, 3524 (2008).

[70]J. R. Jennings, *Catalytic Ammonia Synthesis: Fundamentals and Practice* (Springer Science & Business Media, 2013).

[71]F. Bottomley and R. Burns, *A Treatise on Dinitrogen Fixation* (Wiley-Interscience, New York, 1979).

[72]H.-J. Freund, B. Bartos, R. P. Messmer, H. Grunze, H. Kuhlenbeck, and M. Neumann, Surf. Sci. **185**, 187 (1987).

[73]M.-C. Tsai, U. Ship, I. C. Bassignana, J. Küppers, and G. Ertl, Surf. Sci. **155**, 387 (1985).

[74]J. J. Mortensen, L. B. Hansen, B. Hammer, and J. K. Nørskov, J. Catal. **182**, 479 (1999).

[75]J. J. Mortensen, M. V. Ganduglia-Pirovano, L. B. Hansen, B. Hammer, P. Stoltze, and J. K. Nørskov, Surf. Sci. **422**, 8 (1999).

[76]H. A. Duarte, D. R. Salahub, T. Haslett, and M. Moskovits, Inorg. Chem. **38**, 3895 (1999).

[77]T. L. Haslett, S. Fedrigo, K. Bosnick, M. Moskovits, H. A. Duarte, and D. Salahub, J. Am. Chem. Soc. **122**, 6039 (2000).

[78]B. Chen, G. L. Gutsev, W. Sun, X. Kuang, C. Lu, L. G. Gutsev, S. M. Aldoshin, and B. R. Ramachandran, Phys. Chem. Chem. Phys. **23**, 2166 (2021).

[79]I. Swart, F. M. F. de Groot, B. M. Weckhuysen, P. Gruene, G. Meijer, and A. Fielicke, J. Phys. Chem. A **112**, 1139 (2008).

[80]D. M. Kiawi, V. Chernyy, J. Oomens, W. J. Buma, Z. Jamshidi, L. Visscher, L. B. F. M. Waters, and J. M. Bakker, J. Phys. Chem. Lett. **7**, 2381 (2016).

[81]S. K. Loh, D. A. Hales, L. Lian, and P. B. Armentrout, J. Chem. Phys. **90**, 5466 (1989).

[82]S. Dillinger, J. Mohrbach, J. Hewer, M. Gaffga, and G. Niedner-Schatteburg, Phys. Chem. Chem. Phys. **17**, 10358 (2015).

[83]J. Mohrbach, J. Lang, S. Dillinger, M. Prosenc, P. Braunstein, and G. Niedner-Schatteburg, J. Mol. Spectrosc. **332**, 103 (2017).

[84]J. Mohrbach, S. Dillinger, and G. Niedner-Schatteburg, J. Phys. Chem. C **121**, 10907 (2017).

[85]S. Dillinger, J. Mohrbach, and G. Niedner-Schatteburg, J. Chem. Phys. **147**, 184305 (2017).

[86]M. P. Klein, A. A. Ehrhard, J. Mohrbach, S. Dillinger, and G. Niedner-Schatteburg, Top. Catal. **61**, 106 (2018).

[87]S. Dillinger, M. P. Klein, A. Steiner, D. C. McDonald, M. A. Duncan, M. M. Kappes, and G. Niedner-Schatteburg, J. Phys. Chem. Lett. **9**, 914 (2018).

[88]D. V. Fries, M. P. Klein, A. Steiner, M. H. Prosenc, and G. Niedner-Schatteburg, Phys. Chem. Chem. Phys. **23**, 11345 (2021).

[89]S. Peredkov, M. Neeb, W. Eberhardt, J. Meyer, M. Tombers, H. Kampschulte, and G. Niedner-Schatteburg, Phys. Rev. Lett. **107**, 233401 (2011).

[90]A. Straßner, C. Wiehn, M. P. Klein, D. V. Fries, S. Dillinger, J. Mohrbach, and G. Niedner-Schatteburg, "Cryo spectroscopy of N2 on cationic iron clusters," **155**(23) (in press) (2021).

[91]C. Berg, T. Schindler, G. Niedner-Schatteburg, and V. E. Bondybey, J. Chem. Phys. **102**, 4870 (1995).

[92]S. Maruyama, L. R. Anderson, and R. E. Smalley, Rev. Sci. Instrum. **61**, 3686 (1990).

29 April 2024 06:35:03

[93] D. Proch and T. Trickl, Rev. Sci. Instrum. **60**, 713 (1989).

[94] M. Graf, Diploma thesis, TU Kaiserslautern, 2006.

[95] T. Su and M. T. Bowers, J. Chem. Phys. **58**, 3027 (1973).

[96] T. Su and M. T. Bowers, J. Am. Chem. Soc. **95**, 1370 (1973).

[97] P. Langevin, Ann. Chim. Phys. **5**, 245 (1905); available at (open access): https://gallica.bnf.fr/ark:/12148/bpt6k34935p/f242.item.

[98] T. Su and M. T. Bowers, Int. J. Mass Spectrom. Ion Phys. **12**, 347 (1973).

[99] G. Kummerlöwe and M. K. Beyer, Int. J. Mass Spectrom. **244**, 84 (2005).

[100] D. Roy, R. Robles, and S. Khanna, J. Chem. Phys. **132**, 194305 (2010).

[101] P. Bobadova-Parvanova, K. A. Jackson, S. Srinivas, M. Horoi, C. Köhler, and G. Seifert, J. Chem. Phys. **116**, 3576 (2002).